Chapter 3. Electrical and Optical Characteristics of GaSb

3.1 Introduction

The Hall effect, in particular, has formed one of the essential characterization techniques throughout the history of semiconductor development and this seems likely to continue for the foreseeable future. The reason is that, for an extrinsic semiconductor, it gives a direct measure of free carrier type and concentration which, when combined with a resistivity measurement on the same sample, also yields a value for the appropriate carrier mobility. Knowledge of the electron or hole mobility provides an immediate indication of material quality but, more specifically, experimental data on Hall effect and resistivity over a wide temperature range (4-300 K) can be analyzed to give information concerning impurities, imperfections, uniformity, scatting mechanisms, etc. which is not available from any other single technique. Though special samples are required, they are not difficult to prepare and the measurements make only modest demands on experimental equipment.

Many properties of semiconductors that relate directly to impurities or defects can be assessed by electrical measurements. Such measurements include current-voltage, capacitance-voltage, magnetoresistance, and impedance measurements. Measuring the electrical conductivity of semiconductors as a function of temperature, the intrinsic and extrinsic ranges can be observed. In the intrinsic range (high temperature), the temperature dependence of the conductivity is characteristic of the material itself, in the extrinsic range the density of free carriers is controlled very sensitively by defects or impurities. So this measurement may use to characterize the properties of defects and impurities.

3.2 Experimental details

Hall measurement were done on undoped and Te doped GaSb epilayer grown on SI-GaAs substrates, substrate temperature is measured by a thermocouple calibrated from the GaAs oxide removal temperature (590 °C). GaSb was grown with substrate temperature in the range 460-530°C. Sb_4:Ga beam equivalent pressure ratio was selected around 6. A GaSb growth rate of 1 μm/h was used, and all samples with a 3 μm epilayer. We used the Van der Pauw geometry with four In dots alloyed at the corners of the sample as described earlier. The measurements were done over a range of temperature 4.2-400 K by using the liquid He cryostat. The samples was mounted with vacuum grease on the mica sheet placed on the sample holder for electrical insulation. The Ohmic contacts for four points were bonded Au wire to the pads which were connected through leads to a combination selector.

3.3 Theoretical analysis

3-3.1 Solution of the equations of motion

In practice we are always concerned with a distribution of carrier under the influence of both electric and magnetic fields so we now consider the full equation of motion appropriate to the situation illustrated in Fig. 3-1. We treat the flow of a positive hole current along the positive direction of z and we assume bands with spherical constant energy surfaces. Writing expressions for the component forces acting on the holes in the z and y directions results in:

$$\dot{v}_z = F_z / m^* = \frac{e}{m^*} E_z - \frac{eB_x}{m^*} v_y = \frac{e}{m^*} E_z - \omega_c v_y \qquad (3.3\text{-}1)$$

$$\dot{\upsilon}_y = F_y / m^* = \frac{e}{m^*} E_y + \omega_c \upsilon_z \qquad (3.3\text{-}2)$$

where ω_c is the cyclotron frequency. We wish to solve these equation for the drift velocities υ_y and υ_z so as to obtain expressions for the longitudinal and transverse currents J_z and J_y. We assume, for the moment, that scattering is independent of carrier energy, though, because of the random nature of the scattering process, it is necessary to take an average over the individual collision times. The solution was gives by[2]

$$J_z = \frac{pe^2}{m^*}\left\{\frac{\tau}{1+\omega_c{}^2\tau^2} E_z - \frac{\omega_c{}^2\tau^2}{1+\omega_c{}^2\tau^2} E_y\right\} \qquad (3.3\text{-}3)$$

$$J_y = \frac{pe^2}{m^*}\left\{\frac{\tau}{1+\omega_c{}^2\tau^2} E_y - \frac{\omega_c{}^2\tau^2}{1+\omega_c{}^2\tau^2} E_z\right\} \qquad (3.3\text{-}4)$$

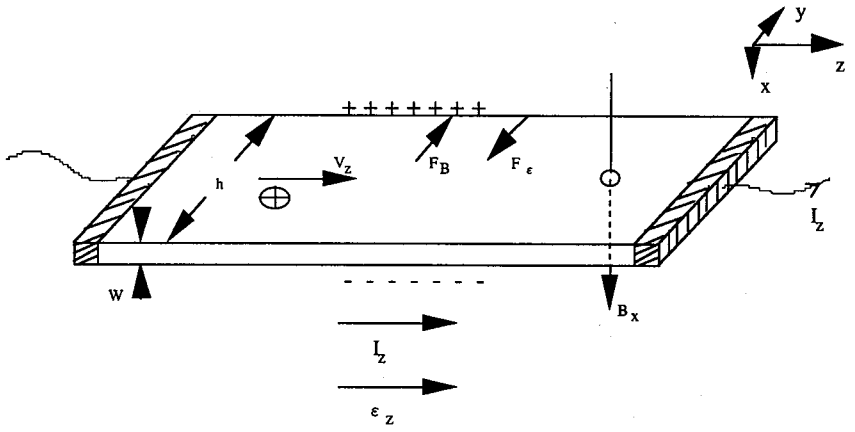

Fig. 3-1 Schematical diagram to illustrate the Hall effect on semiconductor sample in the form of a "Hall bar".

3-3.2 Energy-dependent relaxation time

Accurate interpretation of electrical transport measurement requires one to take account of the energy distribution of free carriers. This arises essentially because the relaxation time τ is generally not constant, as assumed above, but depends on carrier energy E. Therefore, in writing expressions for mobility, conductivity and Hall coefficient one must take account of this energy dependence by averaging over all electron energies. What this implies in practice can be seen by returning to Equations (3.3-3) and (3.3-4) which must now be written:[3]

$$J_z = \frac{pe^2}{m^*}\left\{\left\langle\frac{\tau}{1+\omega_c{}^2\tau^2}\right\rangle E_z - \left\langle\frac{\omega_c{}^2\tau^2}{1+\omega_c{}^2\tau^2}\right\rangle E_y\right\} \qquad (3.3\text{-}5)$$

$$\equiv \sigma_{zz}E_z + \sigma_{zy}E_y$$

$$J_y = \frac{pe^2}{m^*}\left\{\left\langle\frac{\tau}{1+\omega_c{}^2\tau^2}\right\rangle E_y - \left\langle\frac{\omega_c{}^2\tau^2}{1+\omega_c{}^2\tau^2}\right\rangle E_z\right\} \qquad (3.3\text{-}6)$$

$$\equiv \sigma_{yy}E_y + \sigma_{yz}E_z$$

where the bracket $\langle\ \rangle$ implies an average over carrier energy which we define below

i.e., for some function $f(\tau)$

$$\langle f(\tau)\rangle = \frac{\int_0^\infty f(\tau)E^{3/2}\dfrac{\partial f}{\partial E}dE}{\int_0^\infty E^{3/2}\dfrac{\partial f}{\partial E}dE} \qquad (3.3\text{-}7)$$

Here we have extended the upper integration limit to infinite, since $\langle\partial f/\partial E\rangle$ fall off well before the band maximum in all practical case. Note that $\partial f/\partial E$ can be written as $-f(1-f)/kT$, since

$$f = 1/\left[1+\exp\left(E-E_F\right)/kT\right] \qquad (3.3\text{-}8)$$

For nondegenerate electrons (Boltzman statistics), $\partial f/\partial E \cong (kT)^{-1}\exp\left(E-E_F\right)/kT$

since $\exp(E_F - E)/kT >> 1$. For degenerate electrons (Fermi-Dirac statistics), on other hand, and *f(1-f)* is a sharply peaked function, having a value of unity at $E = E_F$, and zero otherwise, like $\delta(E - E_F)$. Thus, for degenerate electrons $\langle f(\tau)\rangle = f(\tau(E_F))$, and for nondegenerate, $\langle f(t)\rangle$ becomes[1]

$$\langle f(\tau)\rangle = \frac{\int_0^\infty f(\tau)E^{3/2}e^{-E/kT}dE}{\int_0^\infty E^{3/2}e^{-E/kT}dE} \qquad (3.3\text{-}9)$$

To obtain general expressions for J_z from these equation is unduly complicated but we can easily deal with the special cases of low and high magnetic fields. It is easy to see, for example, that when $\omega_c^2\tau^2 << 1$ and $J_y = 0$ the conductivity σ is given by

$$\sigma = \frac{pe^2}{m^*}\langle\tau\rangle \qquad (3.3\text{-}10)$$

whereas in high field when $\omega_c^2\tau^2 >> 1$.

$$\sigma = \frac{pe^2}{m^*}\langle 1/\tau\rangle^{-1} \qquad (3.3\text{-}11)$$

Of more immediate interest is the Hall scattering factor r_H which can be obtained from Equations(3.3-5),(3.3-6), (3.3-10) and (3.3-11):

$$r_H = \frac{\left\langle \frac{\tau^2}{1+\omega_c^2\tau^2} \right\rangle}{\left\langle \frac{\tau}{1+\omega_c^2\tau^2} \right\rangle^2 + \omega_c^2\left\langle \frac{\tau^2}{1+\omega_c^2\tau^2} \right\rangle^2} \qquad (3.3\text{-}12)$$

At high magnetic field where $w_c^2\tau^2 >> 1$ it is easy to see that. r_H=1. At low fields where $\omega_c^2\tau^2 << 1$ we obtain:

$$r_H = \langle\tau^2\rangle/\langle\tau\rangle^2 \qquad (3.3\text{-}13)$$

Finally, for a degenerate electron (or hole) gas, $\tau = \tau(E_F)$=constant, so far this case too, r_H=1.

For several scattering processes it is possible to write, at least approximately, $\tau = aE^s$ where a and σ are constant. In such a case, $\langle f(\tau) \rangle$ is straightforward to perform the averaging in terms of the gamma function $\Gamma(p)$:

$$\Gamma(p) = \int_0^\infty x^{p-1} e^{-x} dx \qquad (3.3\text{-}14)$$

and has the property $\Gamma(p+1)=p\Gamma(p)$, for any value of p; $\Gamma(p)=(p-1)!$, if p is an integer; and $\Gamma(1/2)=\pi^{1/2}$. Thus, the commonly encountered function $\langle \tau \rangle$ and $\langle \tau^2 \rangle$ become

$$\langle \tau \rangle = \frac{\int_0^\infty \tau E^{3/2} e^{-E/kT} dE}{\int_0^\infty E^{3/2} e^{-E/kT}} = \frac{\int_0^\infty aE^{3/2-s} e^{-E/kT} dE}{\int_0^\infty E^{3/2} e^{-E/kT}}$$
$$= a(kT)^{-s} \frac{\Gamma(5/2-s)}{\Gamma(5/2)} \qquad (3.3\text{-}15)$$

$$\langle \tau^2 \rangle = \frac{\int_0^\infty \tau^2 E^{3/2} e^{-E/kT} dE}{\int_0^\infty E^{3/2} e^{-E/kT}} = \frac{\int_0^\infty aE^{3/2-s} e^{-E/kT} dE}{\int_0^\infty E^{3/2} e^{-E/kT}}$$
$$= a^2 (kT)^{-2s} \frac{\Gamma(5/2-2s)}{\Gamma(5/2)} \qquad (3.3\text{-}16)$$

Using these equations for r_H we then have:

$$r_H = \frac{\langle \tau^2 \rangle}{\langle \tau \rangle^2} = \frac{\Gamma(5/2-2s)}{[\Gamma(5/2-s)]^2} \qquad (3.3\text{-}17)$$

As an example, consider acoustic-mode deformation- potential scattering, for which s=1/2; then $r_H=3\pi/8=1.18$. The largest possible value of r_H would occur for ionized-impurity scattering, for which $s=3/2$; in that case, $r_H=315\pi/512$. In practice, however, there is always a mixture of scattering mechanisms, and r_H is almost much less than 1.93 for single-band transport.

3-3.3 Two-band transport

The transport properties of holes in semiconductors are of great interest from both physics and device points of view.[4] The presence of two interacting bands (heavy holes and light holes) of carriers introduces considerable complications into any calculation of holes mobility. The correct way of handing this problem is by solving a set of coupled Boltzman equation.[1] The consequences of two-band transport will be discussed in terms of simple models which have been found to be useful and even accurate. The simplest models results from assuming that heavy holes and light holes are decoupled, except for allowing interband transitions in the determination of scattering rates. For heavy holes has higher state density than light holes, this means, of course, that interband scattering will dominate for light holes, while intraband scattering will dominate for heavy holes.

GaSb has special features of the conduction band structure, the lowest minimum in the conduction band lies at the center of the Brillouin zone (Γ_1), and that there further minima at the (111) zone faces (L_1) at an energy about 85 meV above the Γ_1 minimum and at the (100) zone faces (X_1), 300 to 400 meV above the Γ_1 minimum. The small energy difference between the two lowest minima and much higher density of states in the L_1 minima means that, around and above room temperature, a significant fraction of the electronic carriers will be in the L_1 valleys, with the consequence that the analysis of any Hall data requires the use of a two-valley model.

In the effective-mass approximation, the two band parallel conductivity currents are given by[3]

$$j_{1z} = \sigma_{1zz}E_z + \sigma_{1zx}E_x \qquad (3.3\text{-}18)$$

$$j_{1x} = \sigma_{1xz}E_z + \sigma_{1xx}E_x \qquad (3.3\text{-}19)$$

$$j_{2z} = \sigma_{2zz}E_z + \sigma_{2zx}E_x \qquad (3.3\text{-}20)$$

$$j_{2x} = \sigma_{2xz}E_z + \sigma_{2xx}E_x \qquad (3.3\text{-}21)$$

Where

$$\sigma_{1xx} = \sigma_{1zz} = \frac{p_1 e^2}{m_1^*}\left\langle \frac{\tau_1}{1+\omega_{c1}{}^2\tau_1{}^2} \right\rangle \qquad (3.3\text{-}22)$$

$$\sigma_{1zx} = -\sigma_{1xz} = \frac{p_1 e^2}{m_1^*}\left\langle \frac{\omega_{c1}\tau_1{}^2}{1+\omega_{c1}{}^2\tau_1{}^2} \right\rangle \qquad (3.3\text{-}23)$$

$$\sigma_{2xx} = \sigma_{2zz} = \frac{p_2 e^2}{m_2^*}\left\langle \frac{\tau_2}{1+\omega_{c2}{}^2\tau_2{}^2} \right\rangle \qquad (3.3\text{-}24)$$

$$\sigma_{2zx} = -\sigma_{2xz} = \frac{p_2 e^2}{m_2^*}\left\langle \frac{\omega_{c2}\tau_2{}^2}{1+\omega_{c2}{}^2\tau_2{}^2} \right\rangle \qquad (3.3\text{-}25)$$

Here $\omega_{c1}=eB/m_1{}^*$ and $\omega_{c2}=eB/m_2{}^*$, where e is the electronic charge, positive quantity, and $m_1{}^*$, $m_2{}^*$ are the effective mass of the two band. The total current is simply the sum of the currents in the individual bands:

$$j_x = j_{1x} + j_{2x} = -(\sigma_{1zx} + \sigma_{2zx})E_z + (\sigma_{1zz} + \sigma_{2zz})E_x \qquad (3.3\text{-}26)$$

$$j_z = j_{1z} + j_{2z} = (\sigma_{1zz} + \sigma_{2zz})E_z + (\sigma_{1zx} + \sigma_{2zx})E_x \qquad (3.3\text{-}27)$$

where, in Eqs. (3.3-22), (3.3-23) and (3.3-24) the symmetry relationships among the various σ_{ij} are used. Again, the boundary condition for the Hall effect experiment is j_y=0, giving

$$E_x = \frac{\sigma_{1zx} + \sigma_{2zx}}{\sigma_{1xx} + \sigma_{22xx}} \qquad (3.3\text{-}28)$$

so that, from Eqs. (3.3-27), (3.3-28) and the definition of σ and R_H,

$$\sigma \equiv \frac{J_z}{E_z} = \frac{(\sigma_{1zz} + \sigma_{2zz})^2 + (\sigma_{1zx} + \sigma_{2zx})^2}{(\sigma_{1zz} + \sigma_{2zz})} \qquad (3.3\text{-}29)$$

$$R_H \equiv \frac{E_x}{j_z B} = \frac{1}{B}\frac{(\sigma_{1zx} + \sigma_{2zx})}{(\sigma_{1zz} + \sigma_{2zz})^2 + (\sigma_{1zx} + \sigma_{2zx})^2} \qquad (3.3\text{-}30)$$

We consider low magnetic field $\omega_c^2\tau^2 << 1$, then Eqs.(3.3-22)-(3.3-15) yield

$$\sigma_{1zz} = p_1 e^2 \langle \tau_1 \rangle / m_1^* = e p_1 \mu_1 \qquad (3.3\text{-}31)$$

$$\sigma_{1zx} = (p_1 e^2 / m_1^*)(eB/m_1^*)\langle \tau_1^2 \rangle = e p_1 r_1 B \qquad (3.3\text{-}32)$$

$$\sigma_{2zz} = e p_2 \mu_2 \qquad (3.3\text{-}33)$$

$$\sigma_{2zx} = e p_2 \mu_2^2 r_2 B \qquad (3.3\text{-}34)$$

where r_i are Hall factor. However, there are also contributions to the Hall factors due to anisotropy; these have been found to be r_{al}=0.998 and r_{ah}=0.663 for GaSb.[5] Then Hall factors:

$$r_i = r_{ai} \langle \tau_i^2 \rangle / \langle \tau_i \rangle^2 \qquad (3.3\text{-}35)$$

Also, the hole concentrations in each band are approximately given by:

$$p_1 = p / \left[1 + (m_2/m_1)^{3/2} \right] \qquad (3.3\text{-}36)$$

$$p_2 = p - p_1 \qquad (3.3\text{-}37)$$

The conductivity and Hall coefficient now become

$$\sigma_0 = e(p_1 \mu_1 + p_2 \mu_1) = \sigma_1 + \sigma_2 \qquad (3.3\text{-}38)$$

$$R_H = \frac{r_1 p_1 \mu_1^2 + r_2 p_2 \mu_1^2}{e(p_1 \mu_1 + p_2 \mu_2)^2} = \frac{\sigma_1^2 R_1 + \sigma_2^2 R_2}{(\sigma_1 + \sigma_2)^2} \qquad (3.3\text{-}39)$$

where $\sigma_1 = e p_1 \mu_1$, $\sigma_2 = e p_2 \mu_2$, $R_1 = r_1/p_1 e$, $R_2 = r_2/p_2 e$. Hall factor r_H and Hall mobility μ_H, become[6]

$$r_H = epR$$

$$= \frac{(1+\alpha^{3/2})(r_1 \alpha^{3/2} \beta^2 + r_2)}{(1+\alpha^{3/2}\beta)^2} \qquad (3.3\text{-}40)$$

$$\mu_H = R\sigma$$

$$= \frac{e}{m_1^*} \frac{r_{A1} \langle \tau_1^2 \rangle + \alpha^{1/2} r_{A2} \langle \tau_2^2 \rangle}{\langle \tau_1 \rangle + \langle \tau_2 \rangle \alpha^{-1/2}} \qquad (3.3\text{-}41)$$

where $\alpha = m_1/m_2$, $\beta = \mu_1/\mu_2$, $\mu_i = \frac{e\langle\tau_i\rangle}{m_i^*}$. The subscript 1 always refers to heavy and the subscript 2 to light holes.

3-3.4 Scattering theory

In semiconductors electrons or holes migrate through the crystal with properties determined principally by crystal lattice periodic potential and ionized impurity.

It is known that in the Born approximation the scattering probability per unit time $s(\mathbf{K})$ of an electron under the effect of a disturbance can be written as[7]

$$s_{if}(\mathbf{k}) = \frac{2\pi}{\hbar}\left|I(\mathbf{k}' - \mathbf{k})\right|^2 G(\mathbf{k},\mathbf{k}')\delta(E_{\mathbf{k}} - E_{\mathbf{k}'}) \qquad (3.3\text{-}42)$$

with

$$G(\mathbf{k},\mathbf{k}') = \frac{1}{2}\sum_{s_1,s_2}\left|\int u_{\mathbf{k}'}{}^*(\mathbf{r})u_{\mathbf{k}}(\mathbf{r})d\mathbf{r}\right|^2 \qquad (3.3\text{-}43)$$

where the sum is over spin states, I($\mathbf{k}'$-$\mathbf{k}$) is the ($\mathbf{k}'$-$\mathbf{k}$)-th Fourier coefficient of the perturbing Hamiltonian H', $\mathbf{k}'$ and $\mathbf{k}$ are the electrons wave vectors at the initial and final sates respectively. G($\mathbf{k}$,$\mathbf{k}'$) is computed over the Wigner-Seitz cell, and accounts for the overlap between the periodic parts u($\mathbf{r}$) of the wave functions in the mixing of initial and final Bloch states.

The overlap integral given in (2) depends upon the symmetry properties of the initial and final state wave functions. For electrons, the wave function exhibiting spherical symmetry, the overlap integral is near unity, and this fact reduce the complexity of scattering terms. For holes, the situation is not as simple, and the valence band wave functions for cubic structures exhibit a nonspherical symmetry, mostly p-like at the top of band. The overlap integral are dependent on $\mathbf{k}$

and Θ, the angle between **k** and **k'**. Wiley[8] had carried out calculations on G(**k**,**k'**) III-V compounds using the wave functions of Kane.[9] He shown that the overlap functions were not strong functions of **k**, and can be well approximated by their values at **k**=0. In that case

$$G_{h\to l} = G_{l\to h} = 3\left(1-\cos^2\Theta\right)/4 \qquad (3.3\text{-}44)$$

$$G_{h\to h} = G_{l\to l} = \left(1+3\cos^2\Theta\right)/4 \qquad (3.3\text{-}45)$$

3-3.5 Scattering Mechanism

a) Acoustic-mode deformation-potential scattering

The changes in lattice-atom positions due to acoustic-mode lattice vibrations produce a potential that scatters carriers. The scattering rate is[4]

$$s_{if} = \frac{E_1^2 k_B T m_f^*}{\pi\rho\hbar^3 s^2} k_i \int_{-1}^{1} \frac{G(y)}{2} dy \qquad (3.3\text{-}46)$$

where E_1 is the deformation-potential constant, ρ is the mass density of the material, s is the acoustic velocity.

b) Polar optical-mode scattering

The optical-mode lattice vibrations produce a polarization of the ionic charges on neighboring atoms, leading to dipole moments that can interact with the free holes. this is most important scattering mechanism for electrons at room temperature, and is also relatively strong for holes. The scattering rate is[4]

$$s_{if} = \frac{e^2 m_f^* \omega_{po}}{4\pi\varepsilon_0\hbar^2}\left(\frac{1}{\varepsilon_\infty}-\frac{1}{\varepsilon_s}\right)\frac{1}{k_i^2}\left(\sum_{+,-} k_\pm\left(n_0+\frac{1}{2}\mp\frac{1}{2}\right)\right)$$

$$\times\int_{-1}^{1}\frac{G(y)}{\left[1-2(k_{\pm}/k_i)y+(k_{\pm}/k_i)^2\right]}dy \qquad (3.3\text{-}47)$$

where $n_{po}=1/\left[\exp(\hbar\omega_{po}/kT)-1\right]$ and ε_0 is the high frequency dielectric constant. Here, ω_{po} the longitudinal optical phonon angular frequency. The wave vectors $k_{\pm}$ correspond to energies $E\pm\hbar\omega_{po}$, respectively.

c) Nonpolar optical-mode scattering

The following scattering rate for holes by the nonpolar optical-phonon mechanism was derived by D. C. Look *et al.*:[4]

$$s_{if}=\frac{D_K^2 m_f^{3/2}}{2\sqrt{2}\pi\rho\hbar^3\omega_{po}}\sum_{+,-}\left(E\pm\hbar\omega_{po}\right)^{1/2}\left(n_0+\frac{1}{2}\mp\frac{1}{2}\right)\int_{-1}^{1}G(y)dy \qquad (3.3\text{-}48)$$

where D_K is the optical coupling constant, ρ is the mass density of the material.

d) Piezoelectric scattering

The acoustic-mode lattice vibrations produce a potential due to the partial ionization of the atoms in crystals without inversion symmetry. The piezoelectric-potential scattering rate is[10]

$$s_{if}=\frac{e^2h_{pz}^2k_BTm_f^*}{2\pi\rho\hbar^3s^2\varepsilon_\infty^2k_i}\int_{-1}^{1}\frac{G(y)}{2}dy \qquad (3.3\text{-}49)$$

with the piezoelectric constant h_{pz},

3-3.6 Scattering relaxation times

The material parameters are shown in Table I.[11] The relaxation times for various scattering processes can be calculated using above described equations. These values τ_{12}(from heavy to light hole band), τ_{11} (from heavy to heavy hole band), τ_{21} (from light to heavy hole band), τ_{22} (from light to light hole band) are shown in Fig. 3-2 ~ Fig.3-5.

3-3.7 Mobility and Hall factor

A quantitative analysis of the scattering rates for the various lattice scattering processes allows us to compute a drift mobility without scattering by ionized impurities. The correct averaging over the energy is often neglected and substituted by the so called Matthiessen's rule. This approximation is only valid if all relaxation time are independent of the energy or if they would have the same energy dependence.

The energy-averaged values of the relaxation times $\langle\tau_1\rangle$ and $\langle\tau_2\rangle$ and of the squares of the relaxation times $\langle\tau_1^2\rangle$ and $\langle\tau_2^2\rangle$ in both hole bands are needed for the determination of the Hall factor r_1 and r_2. The averaging various scattering processes in the two hole band was performed according to

$$\langle\tau_i\rangle = \frac{4}{3\pi^{1/2}}\int_0^{\infty}\left(\sum_{k=1}^{n}\tau_k^{-1}\right)^{-1}\frac{E^{3/2}}{(k_BT)^{5/2}}e^{-E/k_BT}dE \qquad (3.3\text{-}50)$$

$$\langle\tau_i^2\rangle = \frac{4}{3\pi^{1/2}}\int_0^{\infty}\left(\sum_{k=1}^{n}\tau_k^{-1}\right)^{-2}\frac{E^{3/2}}{(k_BT)^{5/2}}e^{-E/k_BT}dE \qquad (3.3\text{-}51)$$

where $\tau_k^{-1} = s_{ii}^k + s_{ij}^k$.

The temperature dependence of the Hall factors and Hall mobility for the different phonon scattering processes are shown in Fig. 3-6 ~ Fig. 3-7. If we know the single lattice scattering

rates, we can calculate the lattice drift mobility and Hall factor, the lattice Hall mobility and Hall factor as functions of temperature are shown in Fig. 3-8.

3-3.8 Ionized impurities scattering processes

The ionized impurity scattering rate for holes can be readily obtained by considering impurity centers with a screened Coulomb potential is given by

$$s_{if} = \frac{N_I V_c^2}{8\pi^3} \int \frac{2\pi}{\hbar} \frac{e^2}{\varepsilon_s^2 V_c^2} \frac{G(y)(1-y)}{\left[\left|\mathbf{k}-\mathbf{k}'\right|^2 + \lambda_D^{-2}\right]^2} \delta\left(E_{\mathbf{k}} - E_{\mathbf{k}'}\right) d\mathrm{K}' \qquad (3.3\text{-}52)$$

$$d\mathbf{k}' = k' \sin\theta d\theta d\phi dk'$$

$$\left|\mathbf{k}-\mathbf{k}'\right|^2 = k^2 + k'^2 - 2kk'\cos\theta$$

The integration over ϕ gives a factor 2π, and the $\delta\left(E_{\mathrm{K}} - E_{\mathrm{K}'}\right)$ implies that

$$\hbar^2 k_f^2 / 2m_f^* = \hbar^2 k_i^2 / 2m_i^*$$

$$k_f^2 / k_i^2 = m_f^* / m_i^*$$

$$s_{if} = \frac{N_i e^4 m_f^* k_f}{2\pi\varepsilon^2 \hbar^3 k_i^4} \int_{-1}^{1} \frac{(1-y)G(y)}{\left[1 + m_f^*/m_i^* - 2\left(m_f^*/m_i^*\right)^{1/2} y + \lambda_D^{-2} k_i^{-2}\right]^2} dy \qquad (3.3\text{-}53)$$

The lattice mobility has been calculated in the previous section. The concentration of ionized acceptor N_A^- is given in following relation: $N_A^- = p(T) + N_D^+$. The donor impurities are all ionized ($N_D^+ = N_D$). Therefore, the concentration of ionized impurities is:

$$N_A^- = p(T) + 2N_D \qquad (3.3\text{-}54)$$

The contribution of the scattering by ionized impurities into the calculation of effective Hall factor and Hall mobility may be important in the case of undoped GaSb for very wide temperature region, which has a very high unintentional hole concentration grown by all well known growth technique. The determination of the ionized impurity scattering rate is possible if

we know the concentrations of acceptor and donor, and the activation energy of acceptor. The results of temperature dependence of Hall mobility for different acceptor concentrations are shown in Fig. 3-9.

According to above calculation, it is clearly seen that the inclusion of scattering by ionized impurities is important for effective Hall factor and mobility in the case of small hole concentration at low temperatures, and even at high temperature in the case of higher concentrations. In principle, the determination of the ionized impurity scattering rate is possible if the curve of p_H vs. temperature allows a reliable determination of N_a and N_d. However, the parameters N_a and N_d fitted simply from the $P_H(T)$ curve are usual uncertainties, since the effective Hall factor is large and strongly temperature dependent, in addition, the compensation also affect the fitting results. Therefore, an iterative fitting of these parameters is necessary. Such an analysis will be impossible if N_a and N_d cannot be determined reliably as in the case of impurity band conduction.

The commonly made assumption that r_H =1 may often lead to an error of 25% or more in carrier density, an error which can be very much reduced by using the knowledge of r_H now available to us. We first consider value of r_H calculated in the energy independent relaxation approximation for a number of scattering processes, and heavy and light holes are decoupled. In this case, the scattering by deformation potential of optical and acoustic phonons results the Hall factor r_H=1.9. And r_H=4.7 are obtained for polar optical phonon scattering. For scattering by ionized impurities, r_H=1.1 is obtained. The scattering mechanisms mix in real cases and, therefore, the resulting effective Hall factor may be expected to be in the range between 1.9 and 4.7, depending on the relative contributions of the scattering mechanisms. In the high purity materials, scattering by ionized impurities is negligible at room temperature. In the materials of high carrier concentration, scattering by ionized impurities is dominant at large temperature range. The total Hall mobility and the contributions of different scattering mechanisms as a function of temperature are shown in Fig. 3-10.

Table I GaSb physical parameters for the calculation.

Heavy hole effective mass	$0.28\ m_0$
Light hole effective mass	$0.05\ m_0$
Average sound velocity	3.24×10^5 cm/s
Optical deformation potential	6 eV
Acoutical deformation potential	4 eV
Density	5.614 g/cm^3
Static dielectric constant	$(15.0)\varepsilon_0$
High-frequency dielectric constant	$(13.8)\varepsilon_0$
Optical phonon energy	29.9 meV
Piezoelectric constant	0.13 C/m^2
r_{a1}	0.638[a]
r_{a2}	0.998[a]

taken from ref. 11

[a] taken from ref. 5

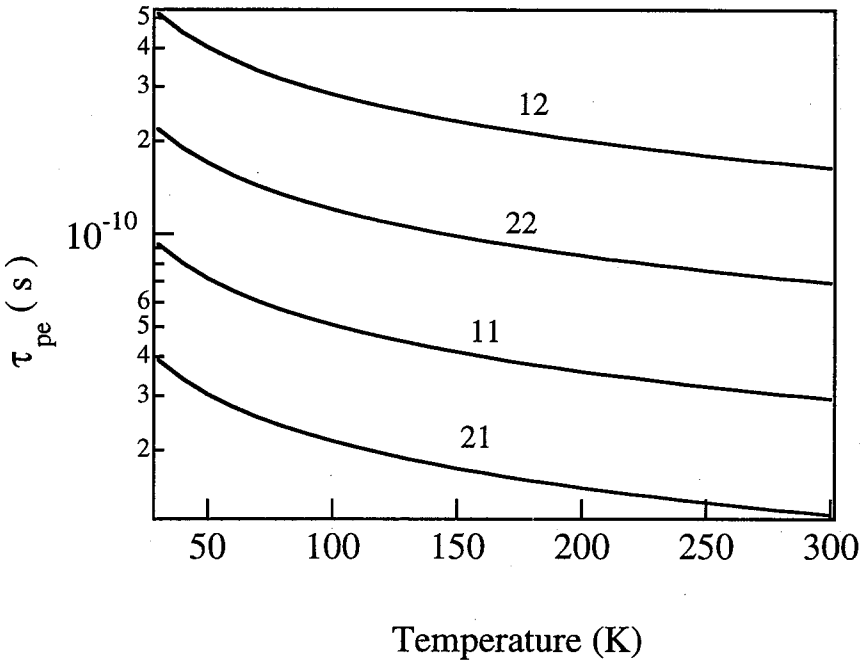

Fig. 3-2 Piezoelectric scattering relaxation times in dependence on temperature.

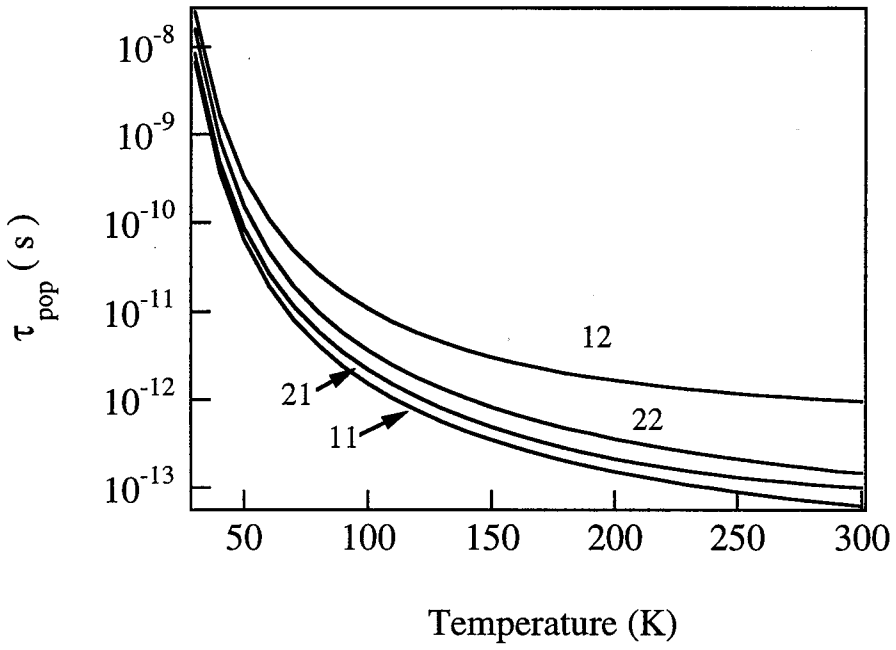

Fig. 3-3 Polar optical phonon scattering relaxation times in dependence on temperature.

11-scattering from the heavy to heavy hole band, 21-scattering from the light hole to heavy hole band, 12- scattering from the heavy to light hole band, and 22-scattering from the light to light hole band.

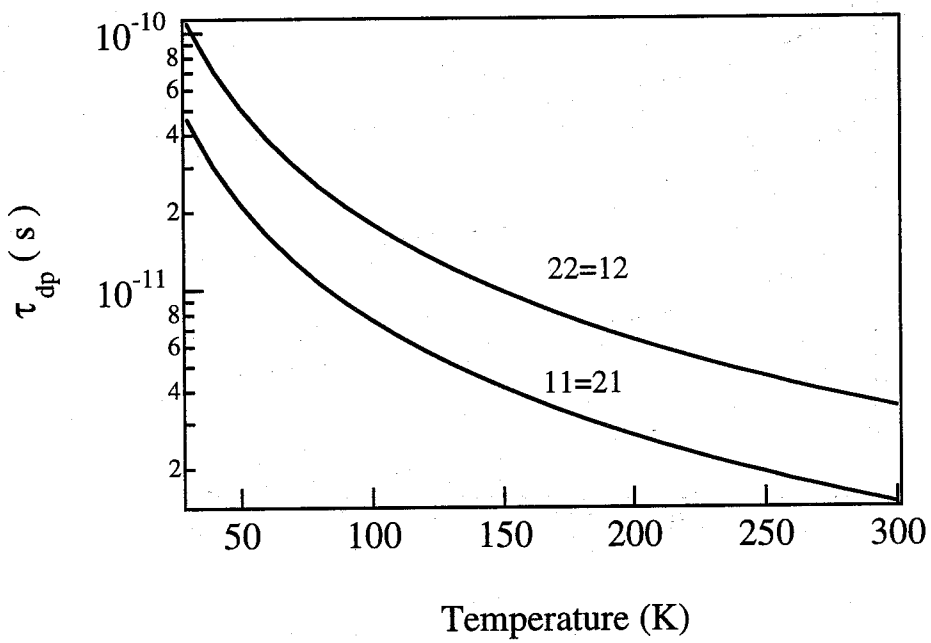

Fig. 3-4 Acoustic phonons scattering relaxation times in dependence on temperature.

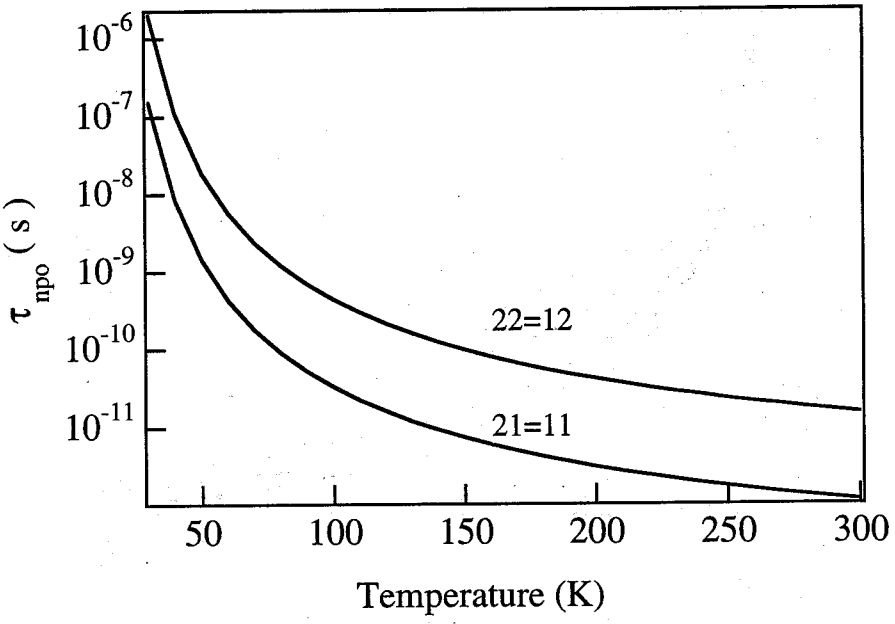

Fig. 3-5 Deformation potential scattering by optical phonon relaxation times in dependence on temperature.

11-scattering from the heavy to heavy hole band, 21-scattering from the light hole to heavy hole band, 12- scattering from the heavy to light hole band, and 22-scattering from the light to light hole band.

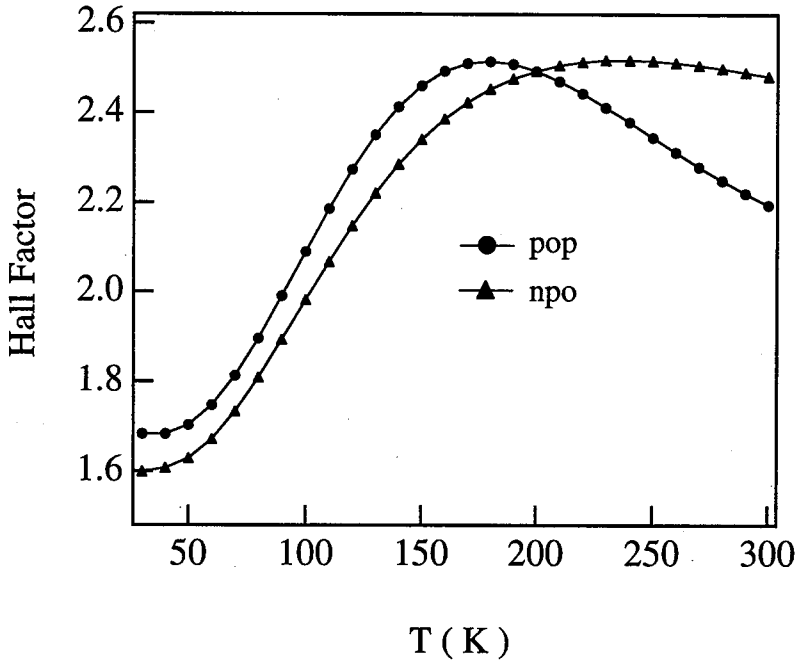

Fig. 3-6 The temperature dependence of the Hall factor for the different phonon scattering processes (r_{ac}=4.4 and r_{pe}=0.906 for all temperatures).

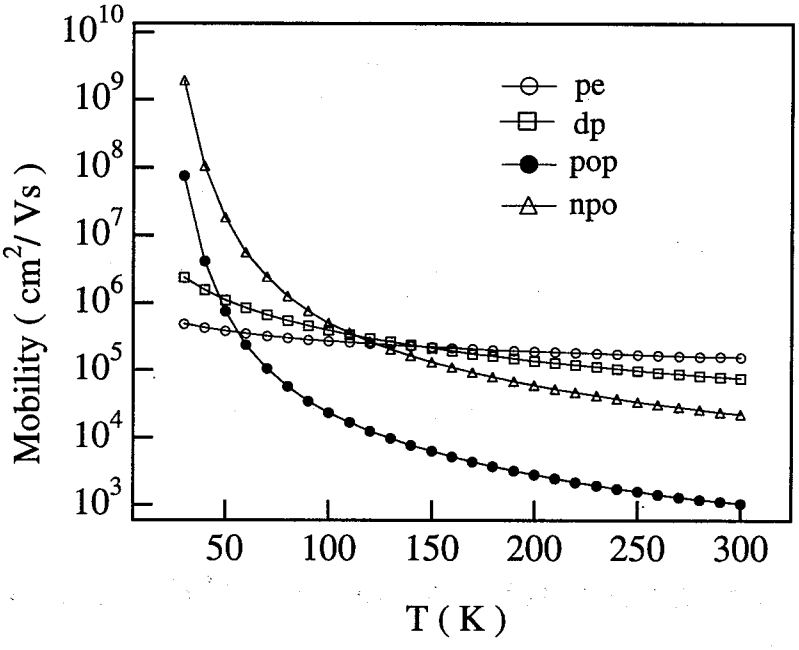

Fig. 3-7 The temperature dependence of the Hall mobility for the different phonon scattering processes.

npo=deformation potential scattering by optical phonons, *dp*=deformation potential scattering by acoustic phonons, *pop*=polar optical phonon scattering, *pe*=piezoelectric scattering.

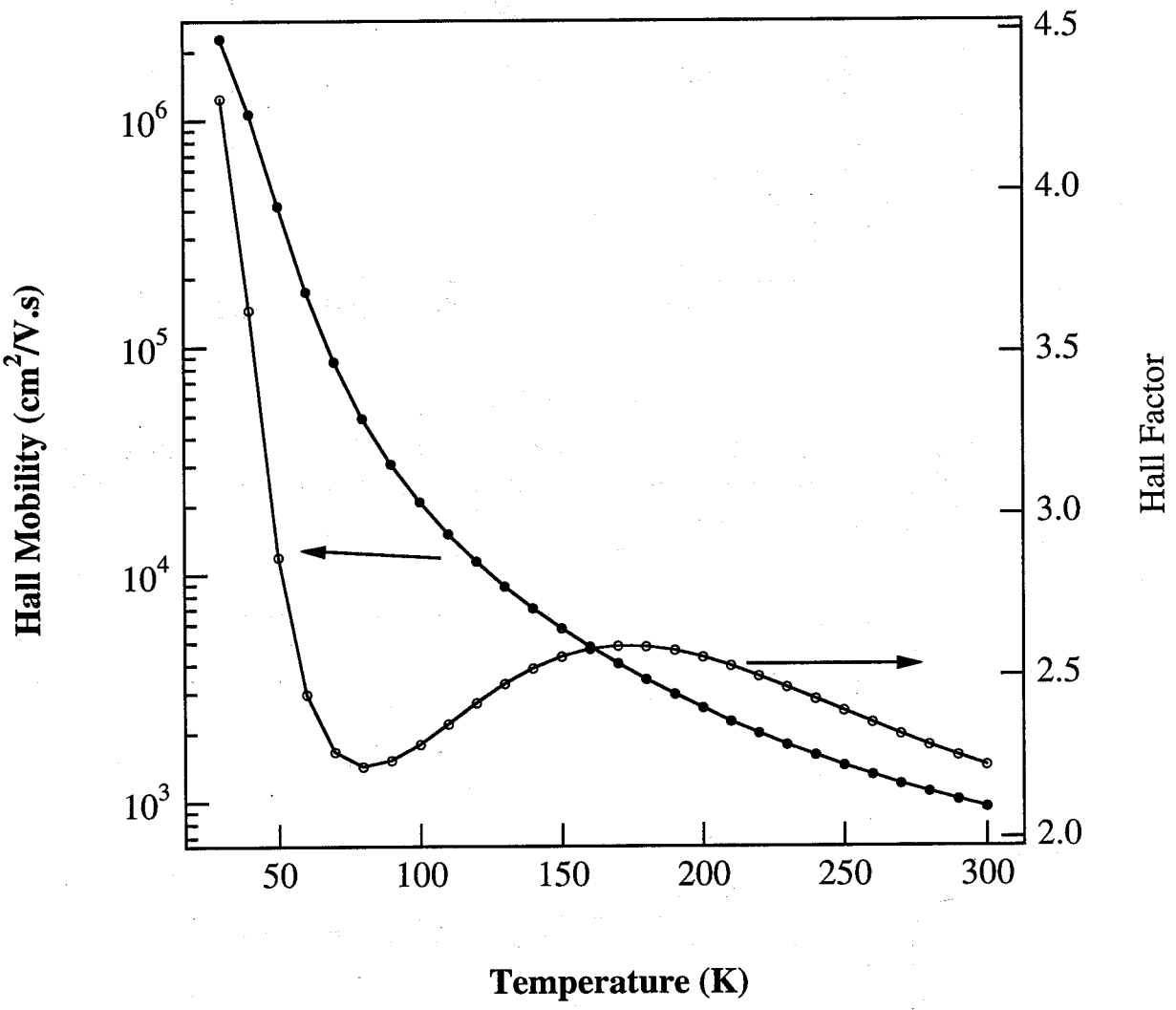

Fig. 3-8 The lattice Hall mobility and Hall factor as functions of temperature.

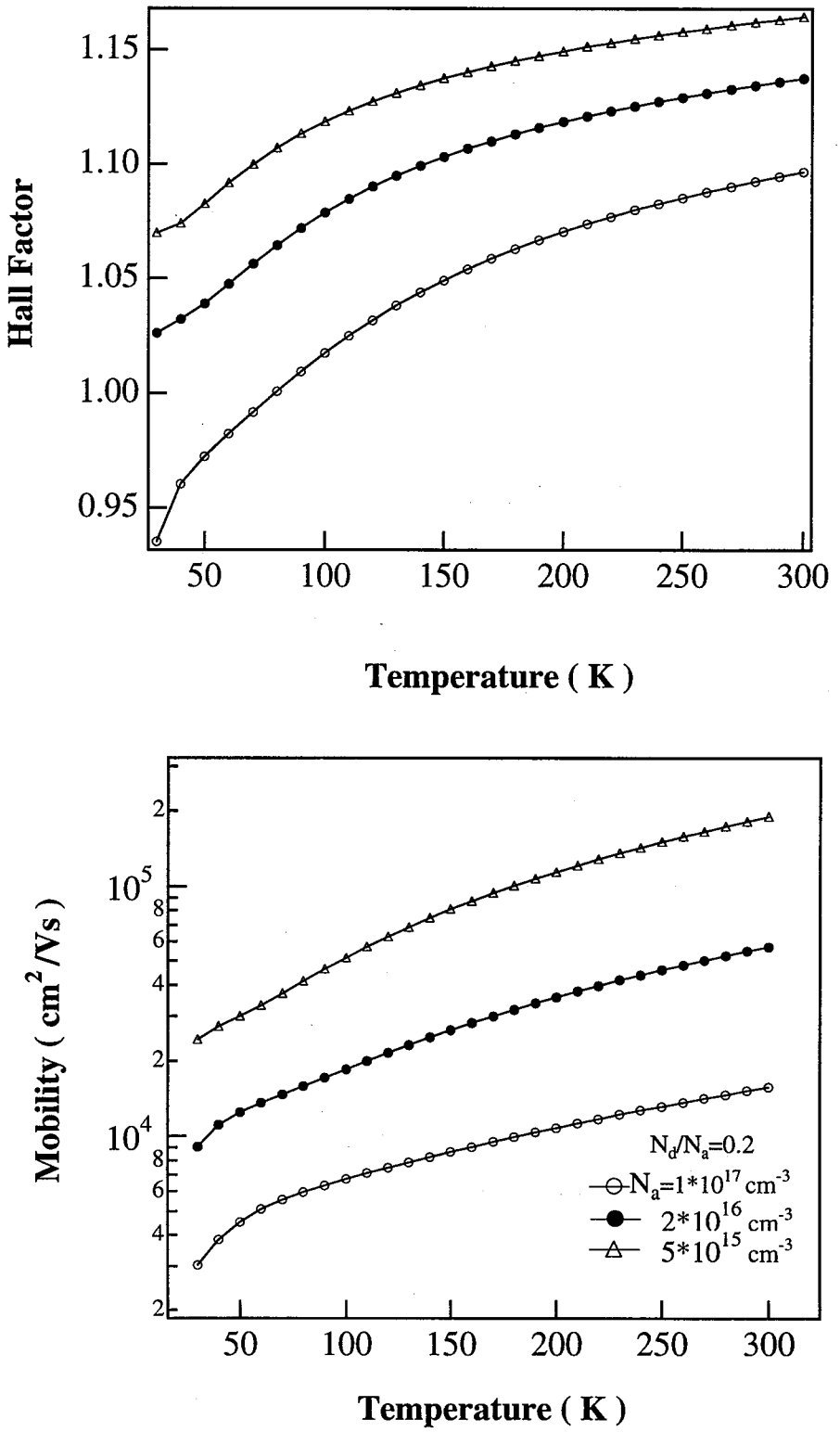

Fig. 3-11 The temperature dependence of Hall factor and mobility for different accepor concentrations

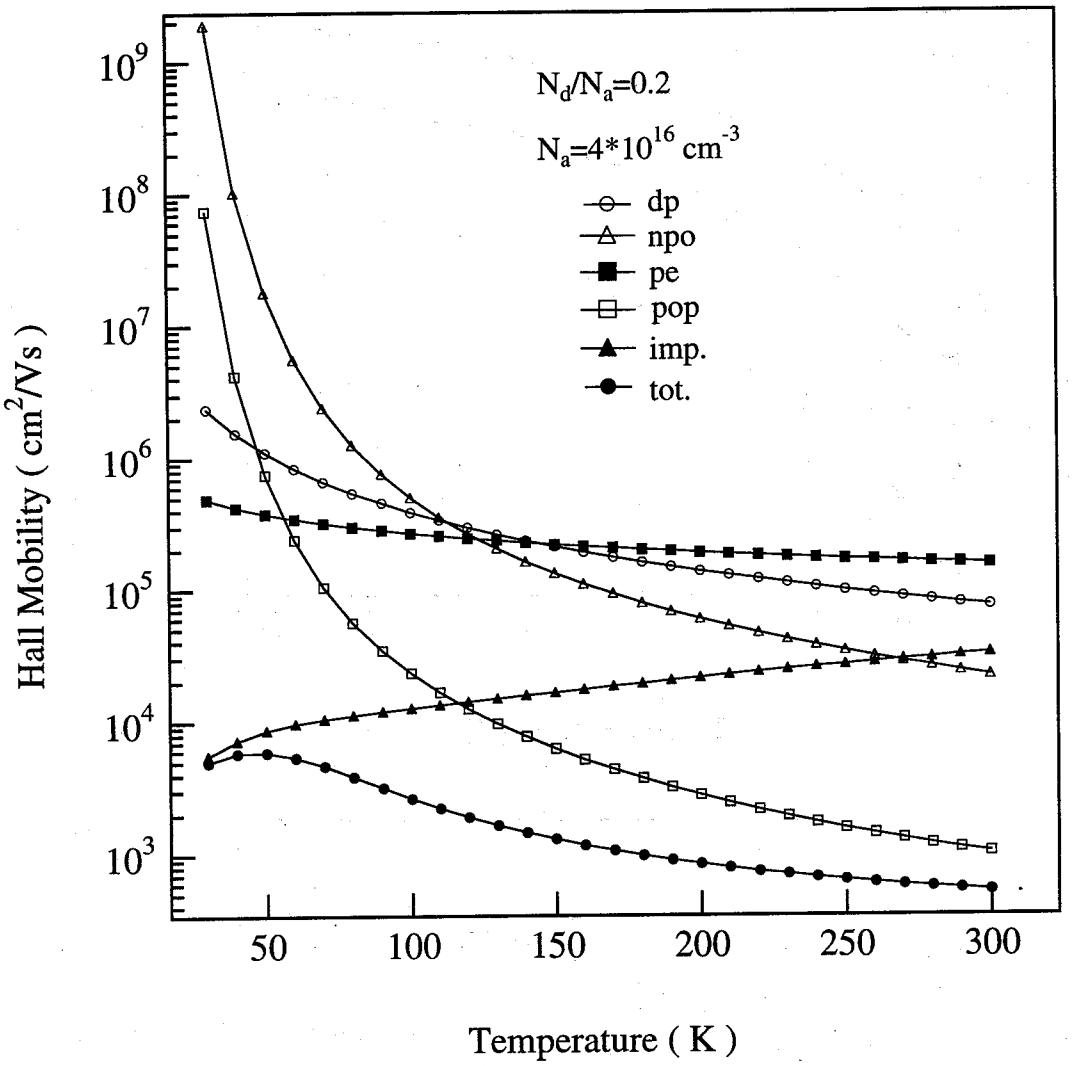

Fig. 3-10 The total Hall mobility and the contributions of different scattering mechanisms as a function of temperature.

3.4. Electrical transport properties of GaSb grown by molecular beam epitaxy

3-4.1. Introduction

In recent years, there has been an increasing interest in GaSb and antimonide based ternary and quaternary compounds because they all have relatively narrow bands, which make them promising materials for photodetectors and medium infrared wavelength range (2-5 μm) lasers.[12] Despite many years of investigations related to Sb-based optoelectronic devices,[12] some problems regarding the growth of device-quality epilayer still persist. The most important one is high unintentionally doped GaSb carrier concentration; it is observed that hole concentration of the order of 10^{17} cm^{-3} is generated in GaSb film grown by standard epitaxal techniques.[12, 13] It has been found that the optical and electrical properties of GaSb are strongly dependent on the growth conditions. Johnson *et al.*[13] found that molecular beam epitaxy (MBE)-grown GaSb epilayers, with the lowest residual acceptor concentrations, do not display the highest hole mobility. This indicates that the transport properties are seriously affected by the compensation effect in undoped *p*-GaSb. But they did not give a detailed study related to the compensated acceptor. In this paper we report a comprehensive analysis and results of transport properties of undoped *p*-type GaSb grown by MBE. Earlier works have mainly concentrated on n-type GaSb, because of its special conduction band structure.[14-17] Recently, Dutta *et al.*[18] studied the hole transport properties of undoped GaSb and GaSb with various degree of tellurium compensation, using Hall measurements. They used the activation energies obtained from PL analysis for determination of concentrations of acceptors and donors. However, it is well known that there are some differences between thermal activation

energy and optical activation energy from as observed PL measurements,[19] and also there are many other unknown fitting parameters which may compensate to each other, leading to some uncertainties in the results obtained by the above method. Therefore, a standard theoretical analysis of Hall data is carried out to study the electrical transport properties of MBE-grown GaSb and the details are described in the subsequent sections.

3-4.2. Experiment

In GaSb epitaxial layer grown on semi-insulating (SI) GaAs substrate by MBE, substrate temperature is measured by a thermocouple calibrated using the GaAs oxide removal temperature (590°C). GaSb was grown with a substrate temperature around 500°C. Sb_4:Ga beam equivalent pressure ratio was around 6. A GaSb growth rate of 1 μm/h was used, and a 3 μm epilayer was formed on all samples.

Hall measurements were performed in the 20 to 340 K temperature range in an Oxford Instruments continuous-flow liquid-helium cryostat using the dc van der Pauw technique. Ohmic contacts on the samples were formed using sintered indium.

3-4.3. Theory

The free hole concentration p and mobility μ of a p-type semiconductor is determined from the measured Hall concentration p_H and Hall mobility μ_H using the following equations:

$$p = r_H p_H \qquad (3.4\text{-}1)$$

$$\mu = \mu_H / r_H \qquad (3.4\text{-}2)$$

where r_H, the effective Hall factor, can be obtained using the relaxation time approximation[4, 6]

$$r_H = \frac{\left[1+\left(m_1^*/m_2^*\right)^{3/2}\right]\left[r_{a1}\left\langle\tau_1^2\right\rangle\left(m_1^*/m_2^*\right)^{-1/2}+r_{a2}\left\langle\tau_2^2\right\rangle\right]}{\left[\left\langle\tau_2\right\rangle+\left\langle\tau_1\right\rangle\left(m_1^*/m_2^*\right)^{1/2}\right]^2} \tag{3.4-3}$$

and the theoretical Hall mobility is given by:[4, 6]

$$\mu_H = \frac{e}{m_1^*}\frac{r_{a1}\left\langle\tau_1^2\right\rangle\left(m_1^*/m_2^*\right)^{-1/2}+r_{a2}\left\langle\tau_2^2\right\rangle}{\left\langle\tau_2\right\rangle+\left\langle\tau_1\right\rangle\left(m_1^*/m_2^*\right)^{-1/2}} \tag{3.4-4}$$

where m_1^* and m_2^* are the heavy and light hole effective masses, respectively, r_{a1} and r_{a2} are anisotropy factors which take into account the anisotropy of the two bands, $\langle\tau_1\rangle$ and $\langle\tau_2\rangle$ are the relaxation times and $\langle\tau_1^2\rangle$, $\langle\tau_2^2\rangle$ are the squares of the relaxation times for heavy and light hole bands, respectively. For the Hall mobility and effective Hall factor calculation, the acoustic-mode deformation potential, acoustic-mode piezoelectric potential, optical-mode deformation potential, optical-mode polar and ionized-impurity screening effects are included. These are similar to those in refs. 4 and 6, but some corrections have been made and are shown in the Appendix. In Table I the material parameters used in the calculation are listed.

For analyzing carrier-concentration vs. temperature data, we assume a nondegenerate semiconductor. Both single acceptor[20~22] and double acceptor[23~25] model proposed by previous researchers. The double acceptor nature of the residual acceptor was first reported by Baxter *et al.*,[23] and Nakashima[24] reviewed all the previous (before 1980) experimental results and showed that the reported ionization energies of such residual acceptors are concentrated around 0.025~0.035 eV and 0.06~0.120 eV respectively, related to the shallow and deep states of the double acceptor. Recently, both single and separated two acceptor model were presented for MBE-grown GaSb.[13, 25] The attempt to analyze the hole concentration with double-acceptor model could not give unique solution. In order to avoid unknown fitting parameters compensate to each other, single acceptor model was used in following analysis. The hole, acceptor and donor concentrations (p, N_a and N_d, respectively) and the activation energy E_a of acceptor are related

through the charge-neutrality condition.[26]

$$\frac{p(N_d + p)}{N_a - N_d - p} = \frac{N_v}{g} exp\left[-\frac{E_a}{kT}\right] \qquad (3.4\text{-}5)$$

where g (= 4) is the acceptor degeneracy factor and N_v is the effective density of states in the valence band. The acceptor and donor concentration, N_a and N_d, respectively, and activation energy E_a may be determined by carrying out a theoretical fit to the experimental data.

In the case of GaSb, where the unintentionally doped hole concentration is of the order of 10^{17} cm^{-3}, large impurity conduction (also known as hopping conductivity) will occur for high impurity concentration at low temperature. This obviously causes a difficulty in the analysis of the Hall measurement data of such a material. Therefore, it is necessary to analyze the mobility versus temperature data to determine N_d.

3-4.4. Results and discussions

The Hall mobility of 3-μm-thick unintentionally doped *p*-type GaSb epilayers, grown at various growth temperatures, is measured at both room temperature and 77 K. A plot of Hall mobility vs. the growth temperature is shown in Fig. 3-11, which exhibits a strong dependence of Hall mobility on the growth temperature. In this report, we will discuss the four samples grown at four different temperatures of 450, 490, 500 and 530°C. Table II summarizes the carrier concentrations and mobilities at both room temperature and 77 K for the GaSb samples, obtained from Hall measurement data.

Figure 3-12 shows plots of the electrical conductivity vs. $1/T$ curves for the four samples mentioned above. The impurity-band hopping conductivity is clearly observed for samples 3 and 4 in the low temperature region. The Hall carrier concentration vs. $1/T$ curves for samples 1, 2 and 3 are shown in Fig. 3-13. For samples 1 and 2, which have higher mobility and are grown at intermediate temperatures, there are two distinct regions in the concentration vs. $1/T$ curves with a

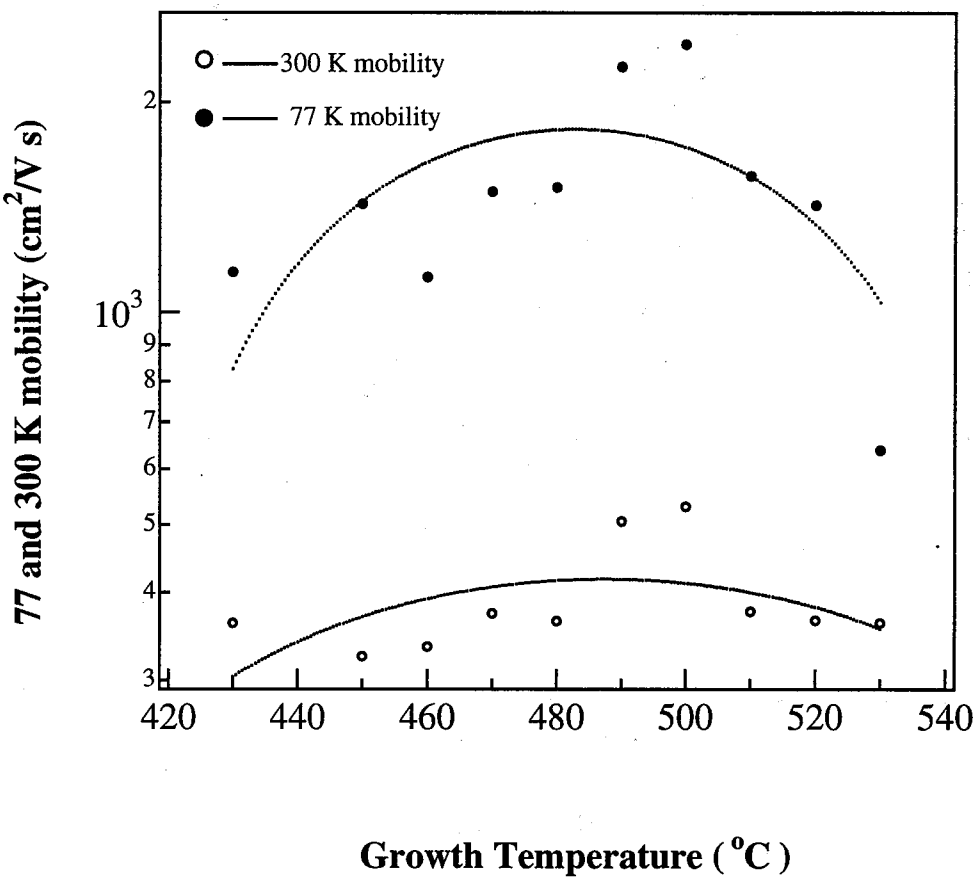

Fig. 3-11 300 and 77 K Hall hole mobility of undoped GaSb layers as a function of growth temperature

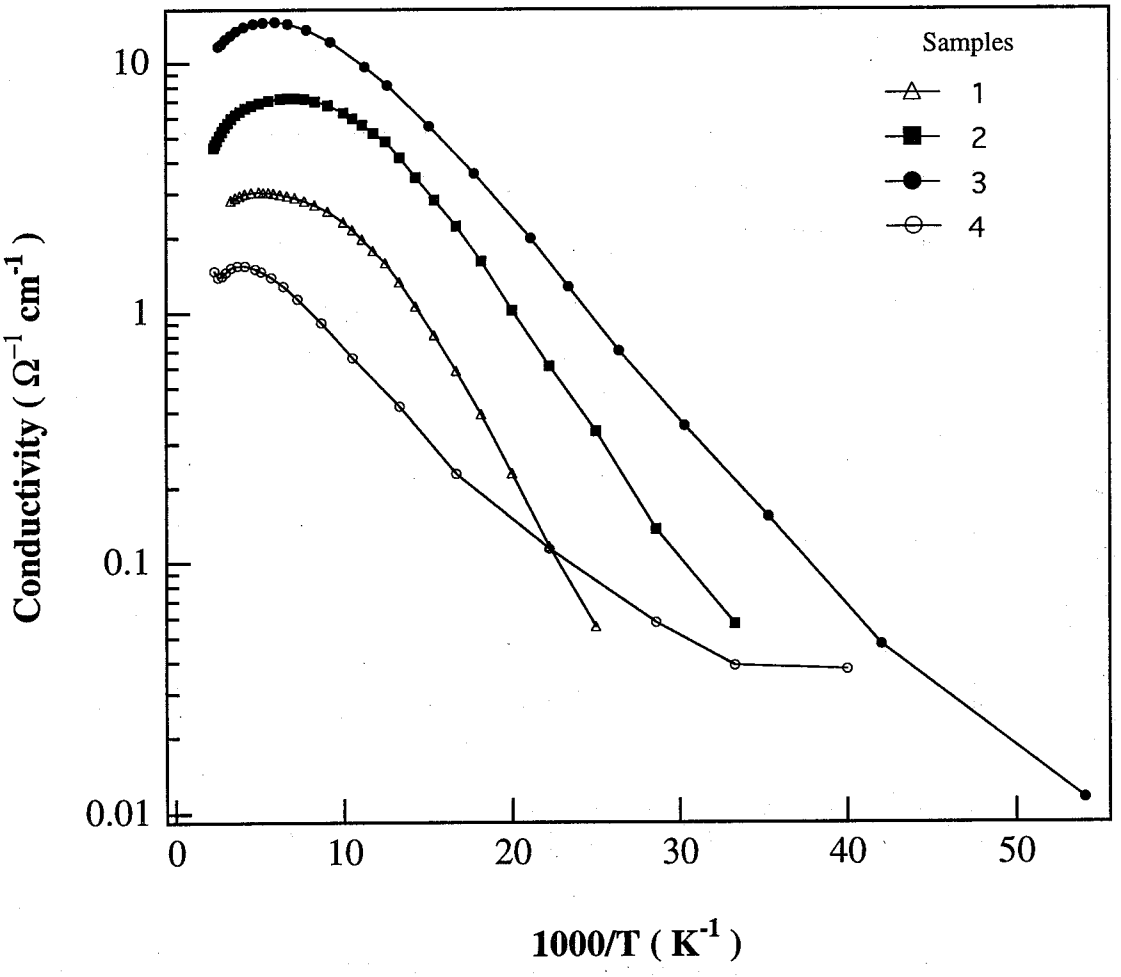

Fig. 3-14 Electrical conductivity vs 1/T plot for samples 1, 2, 3 and 4. (1: 500 °C; 2: 490°C; 3:450°C; 4: 530°C.)

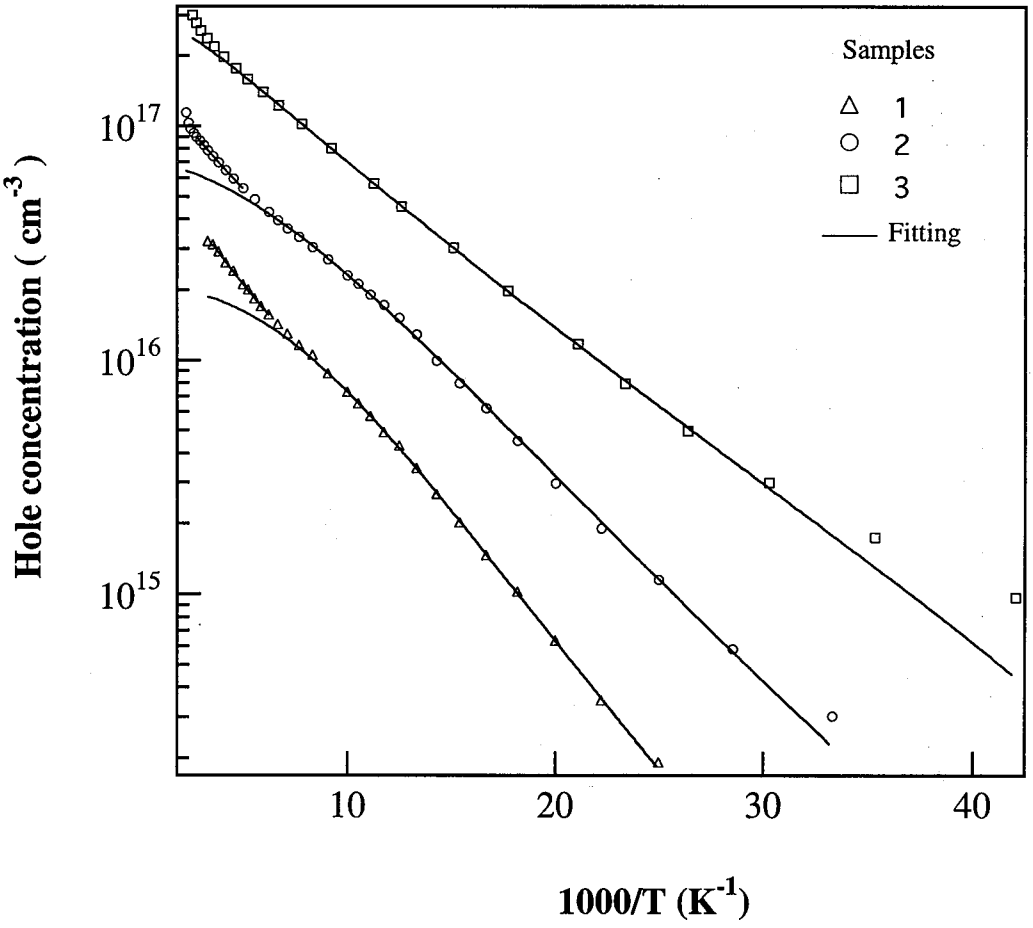

Fig. 3-13 Measured carrier concentrations as a function of temperature for samples 1, 2 and 3. The solid lines represent the best theoretical fits.

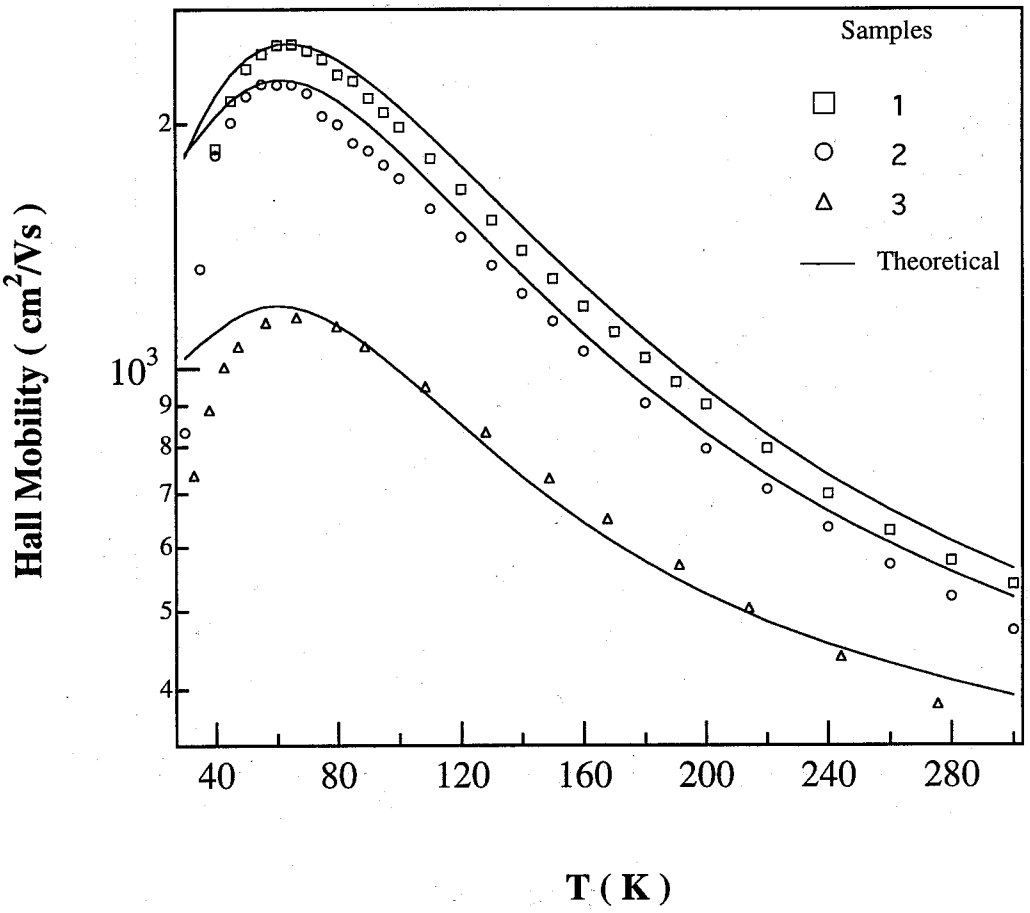

Fig. 3-14 Hole mobilities as a function of temperature for samples 1, 2 and 3. The solid lines represent theoretically calculated Hall mobilities.

noticeable change in gradient (Fig. 3-13), and it is concluded that two separate activation centers are responsible for these two regions. Equation (5) will be applied with different sets of parameters for different temperature regions of the fitting. The model takes account of the temperature dependence of the Hall factor which can introduce significant a error as pointed out by many authors.[6,27] The solid curves in Fig. 3-13 are the results of fitting, and show a good agreement with the experimental data. Using the parameters obtained by fitting, the theoretical Hall mobility is also calculated, and the calculated results are shown in Fig. 3-14. Here too a reasonably good agreement between the theoretical calculation and the experimental data has been obtained (for sample 1 and 2), and the slight deviation between the theoretical fit and experimental data may be partly due to the scattering of the dislocation, because of high lattice mismatch (>7%) between GaAs substrate and GaSb, and partly due to the impurity conduction which may have significant effect on the mobility, especially at a low temperature. This implies that the values of N_a, N_d and E_a obtained by fitting are reliable, and are shown in Table III.

While two energy levels have been obtained for sample 1 (17 and 64 meV) and sample 2 (13 and 67 meV), only one energy level (21 meV) has been obtained for sample 3. The values of activation energy E_{a1} obtained are in the range of 13~21 meV and are close to those obtained by Meinardi *et al.* (15.2~17.6 meV)[25] and Johnson *et al.* (10.5~16 meV).[13] However, the values of activation energy reported by Dutta *et al.* are much higher and are obtained from PL analysis in contrast to those of Meinardi *et al.* and Johnson *et al.* which were obtained from fitting to Hall measurement data, a procedure similar to ours. In general, it is difficult to relate the PL and Hall effect measurement results. Since the electronic transport properties are determined by the defects, these can control the position of the Fermi level, but they may be nonradiation centers. For example, low temperature PL spectra of undoped GaSb exhibits 20 transitions,[28] but only 1~2 activation centers for this material were obtained from Hall data analysis. In ref. 11, the authors used activation energy of PL data (E_{a1}= 31.2, E_{a2}= 102, E_{a3}= 72 meV) for their fitting. For such deep energy levels, impurity potential is strongly localized and the effective mass approximation is

not suitable, and they are not thermally ionized even at room temperature (for E_{a2} and E_{a3}). Therefore the results of Hall effect measurement are not determined by these states. The difference between the thermal activation energy and the optical activation energy can be easily understood using the configuration coordinate diagram of this situation.[19]

For sample 3, grown at a lower temperature, although a good fit can be obtained in 70 to 240 K temperature range for p vs. $1/T$ curve, the theoretical and experimental Hall mobility shows unreasonable deviation. We believe that this is due to some compensated acceptors existing at a shallower level than the principal species with a smaller concentration than the total concentration of all types of donors, which leads to an underestimation of the value of N_d by the standard analyzing process. Therefore, an approximate value of N_d is determined by adjusting its value until a good fit is obtained between the theoretical and experimental Hall mobility vs. temperature plot. The result is also shown in Table III and Fig. 3-14. We observed that the sample 3 shows the lowest donor density. It seems to be a contradictory result. In fact, in order to obtain the exact fitting parameters the self-consistent method should be used (which satisfy both measured Hall mobility and carrier density).

For sample 4, grown at a higher temperature, the impurity conductivity is the dominant conduction process on a large temperature range (below 130 K). The effort to analyze both concentration and mobility from Hall data, using the methods described above, have proved unsuccessful . This has been explained as follows: when the impurity concentration is increased to the level where the average acceptor separation is comparable to the Bohr radius of the ground state, due to an overlap of the ground state wave function the acceptor levels form a band and impurity conduction occurs in parallel with the normal conduction band process. As a result of acceptor freeze-out, impurity conduction may easily become the dominant conduction mechanism. On the other hand, the mutual Coulomb and exchange interactions (the overlap of the ground state wave function) broaden the range of acceptor states, so the activation energy of acceptor is decreased. But, the sample demonstrates lower carrier concentration and mobility, which indicates

that the compensation is so heavy that hole conduction is controlled by deep level acceptors.

It is interesting to study how the Hall mobility versus T curve, shown in Fig. 3-15, alters with an increase in the compensating donor concentration N_d (or compensation ratio N_d/N_a), with N_a and E_a kept constant (a common N_a=10^{17} cm^{-3}, and E_a=12 meV are assumed). Figure 3-16 shows the theoretical calculation of μ(77 K) vs. p(77 K) with the compensation ratio N_d/N_a as a variable parameter. The mobility abruptly decreases with increasing compensation ratio and acceptor concentration. Mobilities of 2000-5000 $cm^2V^{-1}s^{-1}$ for 10^{17}-10^{15} cm^{-3} hole concentrations, at 77 K have been reported by many authors.[29, 30] Comparing these results to the results obtained by theoretical calculations, we can conclude that electrical transport of GaSb is affected by high compensating donor concentration.

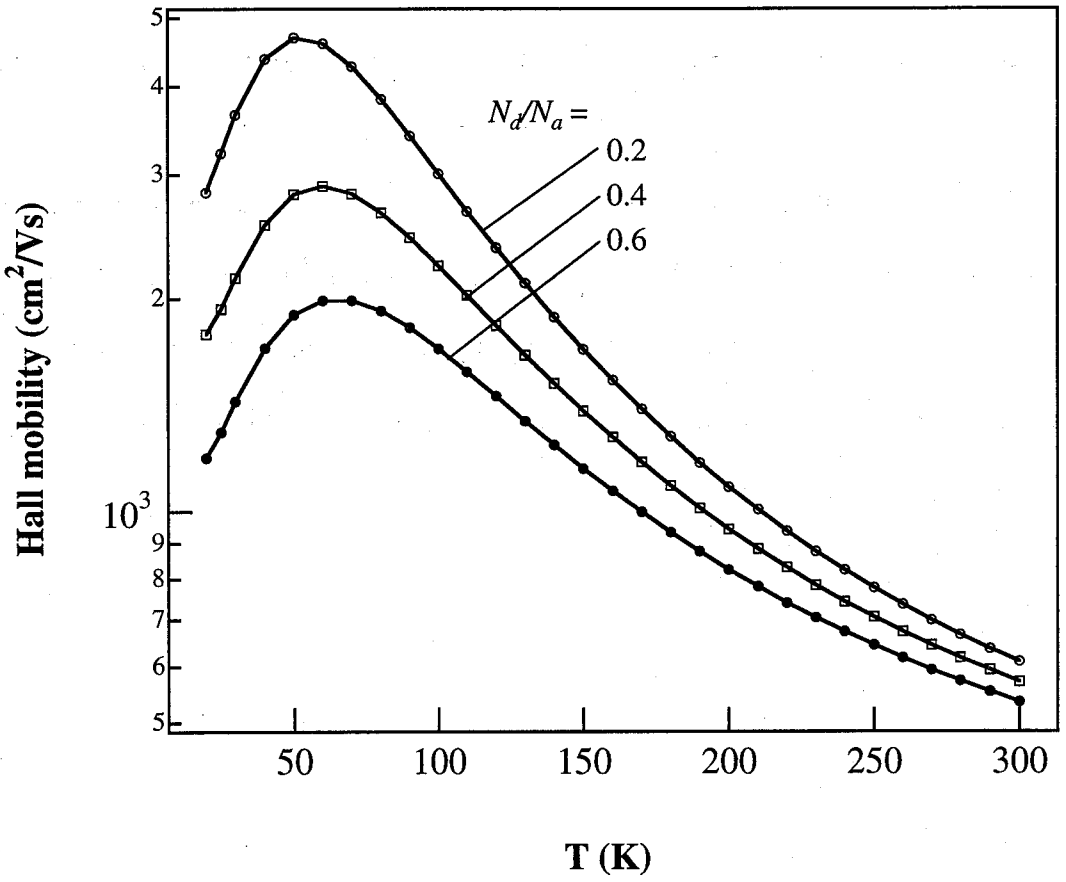

Fig. 3-15 Theeoretically calculated Hall mobilitys showing the temperature dependence of the carrier concentration for various N_d/N_d compensation ratios, and $N_a=1\times10^{17}$ cm^{-3}, E_a=12 meV.

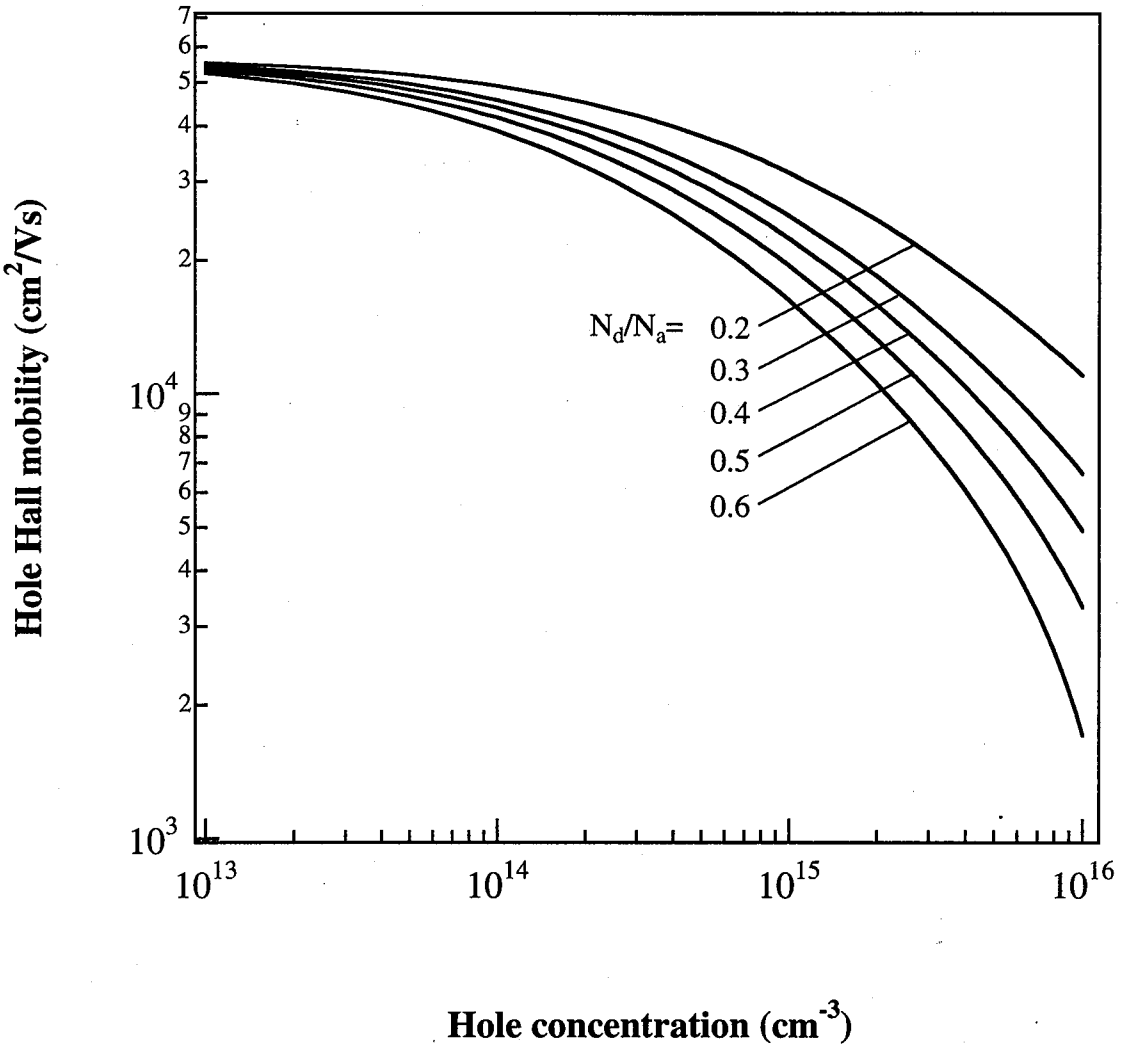

Fig. 3-18 The dependence of Hall mobility on free hole concentration for various compensation at 77 K, while E_a=12 meV

Table II. Hall measurements results at 300 K and 77 K of GaSb growth at various temperatures.

Sample	Growth temperature (^{0}C)	300 K		77 K	
		p (cm^{-3})	μ (cm^2/V s)	p (cm^{-3})	μ (cm^2/V s)
1	500	4.14×10^{16}	530	4.72×10^{15}	2418
2	490	7.0×10^{16}	505	1.2×10^{16}	2242
3	450	2.25×10^{17}	362	4.22×10^{16}	1143
4	530	2.81×10^{16}	317	3.98×10^{15}	638

Table III. Values of parameters obtained by theoretical fitting and calculation for different undoped GaSb samples

Sample	N_{a1} (cm^{-3})	N_{a2} (cm^{-3})	N_d (cm^{-3})	E_{a1} (meV)	E_{a2} (meV)
1	6.7×10^{16}	2.73×10^{16}	4.6×10^{16}	17	64
2	1.65×10^{17}	7.53×10^{16}	6.2×10^{16}	13	67
3	2.8×10^{17}		1.5×10^{16}	21	

3.5 Photoluminescence measurement

Photoluminescence (PL) is a non-destructive spectroscopic technique for analyzing both the intrinsic and the extrinsic properties of semiconductors. PL concerns the radiation emitted by a crystal after optical excitation. In particular, it regards the radiative recombination paths of photoexcited electron-hole pairs. PL provides information mainly on minority carrier properties and, thus, it is complementary to electrical characterization techniques.

PL of undoped bulk GaSb growth from solution has been studied by many authors.[31-36] The unintentionally doped GaSb grown by most epitaxial techniques is naturally *p* type with a hole concentration higher than 1×10^{17} cm^{-3}, and the low-temperature PL was dominated by recombination at the native acceptor via band-acceptor or donor-acceptor pair transitions. The peak energy of this transition was 777.5 meV. When the grown from an Sb-rich melt, the PL was dominated by the band-related transition at 796 meV. All good quality, material also showed a peak at 810 meV corresponding to the free exciton transition, indicating high optical quality. The low-temperature PL spectra of GaSb has been intensively studied, it exhibits many transitions in the energy range of 680-810 meV, listed in Table IV.[37]

The PL spectra were obtained in a 1 m Spex grating spectrometer. The excitation source was the 514 nm line of an Ar^{+} laser, maximum power 500 mW. The normally incident laser beam was focused onto the surface of the sample in a spot. Luminescence was detected using a North Coast germanium detector cooled to 77 K, used with conventional lock-in techniques. The samples immersed in liquid helium at 4.2 K.

Figure 3-17 shows PL spectra obtained from homoepitaxial three samples with different growth temperature. The spectrum are typical of GaSb grown under all antimony stable conditions and

Table IV. Low temperature PL features previously observed in unitentionally doped GaSb. The notation is that used in the literature.

Energy (m eV)	Transition	Notation
810	Free exciton	FE
808.7	Unidentified	
807.95	Unidentified	
805.4	Exciton bound to neutral acceptor	BE1
803.4	Exciton bound to neutral acceptor	BE2
800.1	Exciton bound to neutral acceptor	BE3
796.1	Exciton bound to neutral acceptor	BE4
795	Unidentified	
777.5	Residual acceptor	A
765	LO phonon replica of BE4	BE4 LO
758	Acceptor	B
752	Unidentified	
748.5	LO phonon replica of A	A LO
728	LO phonon replica of B	B LO
722	Unresolved	
710	Second ionization level of acceptor A	C
694	Unidentified	
682	LO phonon replica of C	C LO
680	Unidentified	

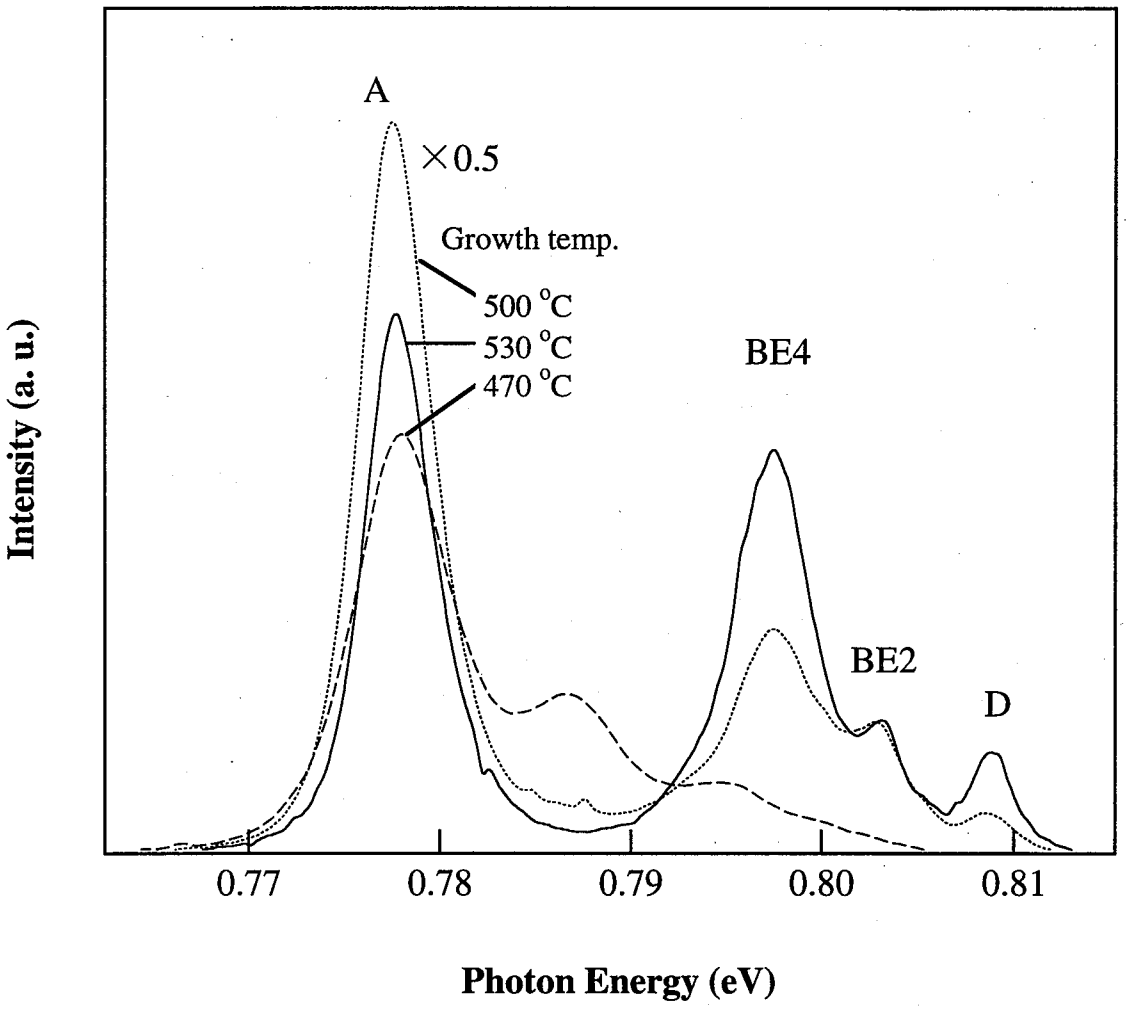

Fig. 3-17 The PL of homoepitaxial GaSb layer showing various transitions observed in good-quality material. (Spectrum taken at 4.2 K)

show the various transitions which have been observed in good quality materials. The dominant recombination mechanism proceeded via the residual acceptor A, at 777.5 meV, for all the samples. It can be seen from the Fig. 3-17 that the spectra obtained from higher growth temperature, a series bound exciton transitions and recombination at the neutral acceptor level as suggested by many author. But we did not observed any phonon replicas for those luminescence. It is worth noting here that the free exciton recombination is not observed in that samples. But a exciton bound to donor (D) is clearly seen, this mean our samples, which grown at higher temperature, have very good crystal quality, because the exciton bound energy is very small for this material. For the sample growth at 500 °C, a strong and narrow A peek is observed, increasing the growth temperature, all transition peaks become weak and broaden. For the sample growth at lower temperature, a unidentified transition located at 786 meV may be due to the free electron to acceptor recombination. The bound exciton recombination BE4 and D did not observe.

3.6 I-V Measurements

3-6.1 Analysis method

I-V measurements are widely used to characterize the barrier height, carrier transport mechanisms, and interface states in Schottky barriers and p-n junctions.[37-39] The extraction of the diode parameters is usually complicated by their voltage and the presence of series resistance. Due to the relative high undoped carrier concentration and narrow band-gap, the leakage current of the GaSb Schottky diodes and p-n junction are relative large. The dark current of a photodetector usually increases with temperature and has to be suppressed in order to operate the photodetectors at high temperature. In addition, for narrow-band gap semiconductors such as

InSb, InAs and GaSb, the surface state due to material or process induced defects may cause serious shunt leakage current.

The current transport in n^+-p rectifying contacts is mainly due to majority carriers. The various current components occurring at p-n junctions are:

1) diffusion currents,

2) space-charge recombination currents,

3) tunneling currents and

4) perimeter currents connected with surface recombination.

At high forward-bias the dominant radiative current is diffusion current, whereas space-charge recombination and tunneling currents contribute little to total current. Perimeter currents involving surface recombination are non-radiative.

The diffusion theory of Shockley[37] predicts the following voltage dependence of the diffusion current density:

$$J = J_0\left[\exp(eV/kT) - 1\right] \qquad (3.6\text{-}1)$$

Experimental observation is made difficult usually by series-resistance effects which influence the *I-V* characteristics at high forward-bias.

Current components due to space-charge recombination become important when recombination centers are present within the space-charge region. By applying Shockley-Read-Hall statistics to space-charge recombination, the following relation can be obtained for the space charge recombination current density:

$$J = J_0\left[\exp(eV/2kT) - 1\right] \qquad (3.6\text{-}2)$$

Surface recombination will occur at the perimeter of a p-n junction, if we define an effective width, L_s, where surface recombination takes place, the perimeter current can be expressed by the surface recombination velocity, s, and the diode perimeter,

$$I_s = sL_s n_i P\left[\exp(eV/nkT) - 1\right] \qquad (3.6\text{-}3)$$

For low bias, the ideality factor in Eq. (3-6.3) is n=2, the same as for bulk space-charge recombination.

At very low bias, temperature-independent slopes may be observed, which is indicative of tunnel or leakage currents. For the tunnel current, we adopt the algebraic equation derived the I-V characteristics of a tunnel diode and may be write it as[39-41]

$$J = J_p\left(V/V_p\right)\exp\left(1 - V/V_p\right) \qquad (3.6\text{-}4)$$

where V_p is the voltage at the maximum forward tunneling current density J_p and V is the applied voltage.

An experimental study of the current flow across p-n junction is easily done by evaluating the slopes in a ln$J$ versus voltage plot at different temperature. By determining the "ideality factor", n, in the exponential relationship.

$$n = \frac{q}{kT}\frac{dV}{d(\ln I)} \qquad (3.6\text{-}5)$$

one can usually differentiate between diffusion current (n=1) observed at high biases, and space-charge recombination current (n=2) at low biases. there are p-n junctions, however, where n lies between 1 and 2.

This "2kT current" is experimentally observed at low biases in the I-V characteristics.

3.6.2 Experiment and results

The GaSb epitaxial layers were grown by MBE on Te doped LEP n-type GaSb (001) substrates. Prior to the growth, substrates were etched lightly by a solution of HF-NHO_3-CH_3COOH, rinsed in de-ionized water, and blow dried. To remove surface oxides, the substrate temperature was raised above 600 °C under Sb_4 flux. After this, a 3 μm undoped GaSb films directly grown on LPE undoped GaSb substrates, then 0.5 μm GaTe-doped n^+-type

GaSb were grown by MBE. Growth temperature was about 500°C with a growth rate of 0.8 μm/h under Sb_4/Ga BEP ratio 6, as measured with an ionization gauge in the growth position. Surface reconstruction during growth was monitored by reflection high-energy electron diffraction (RHEED). Under this growth conditions, a (1×3) pattern was consistently obtained.

Since GaSb surface are easily oxidized, the grown samples were immersed in methanol before processing. Ohmic electrodes with a 150 μm diameter were fabricated by evaporating Au-Ge-Ni alloy on the n-type epilayer through a dotted mask. In was used as the p-type electrode. After the deposition processes, the samples were annealed for 30 s at 300°C in nitrogen atmosphere.

A. Reverse current

The results of reverse currents versus inverse temperature at different biases are shown in Fig. 3-18. The almost constancy of reverse current at low temperature implies the that dominant mechanics at this temperature range is due to tunneling. The tunneling current is caused by electrons tunneling from p-type valence band to n-type conduction band.

At around 300 K, the diffusion current is dominant. The equation for the reverse diffusion current is written as[37]

$$I_R = en_i^2 A_j \left(\frac{D_n}{N_a L_n} + \frac{D_p}{N_d L_p} \right) \exp\left(-\frac{E_g}{kT} \right) \qquad (3.6\text{-}6)$$

where A_j is cross section area, N_a is the p-type acceptor density while N_d is n-type donor density, n_i is the intrinsic carrier concentration, and E_g is the band gap energy of the semiconductor. D represents the diffusion coefficient, and L represent the diffusion length. The band gap energy can be calculated from the slope of log (I_R) vs inverse temperature. The derived band gap energy is 0.8 eV, it is agreement with true value 0.72 eV.

Equation 3.6-4 is used to describe the tunnel current characteristics of our two diodes at reverse

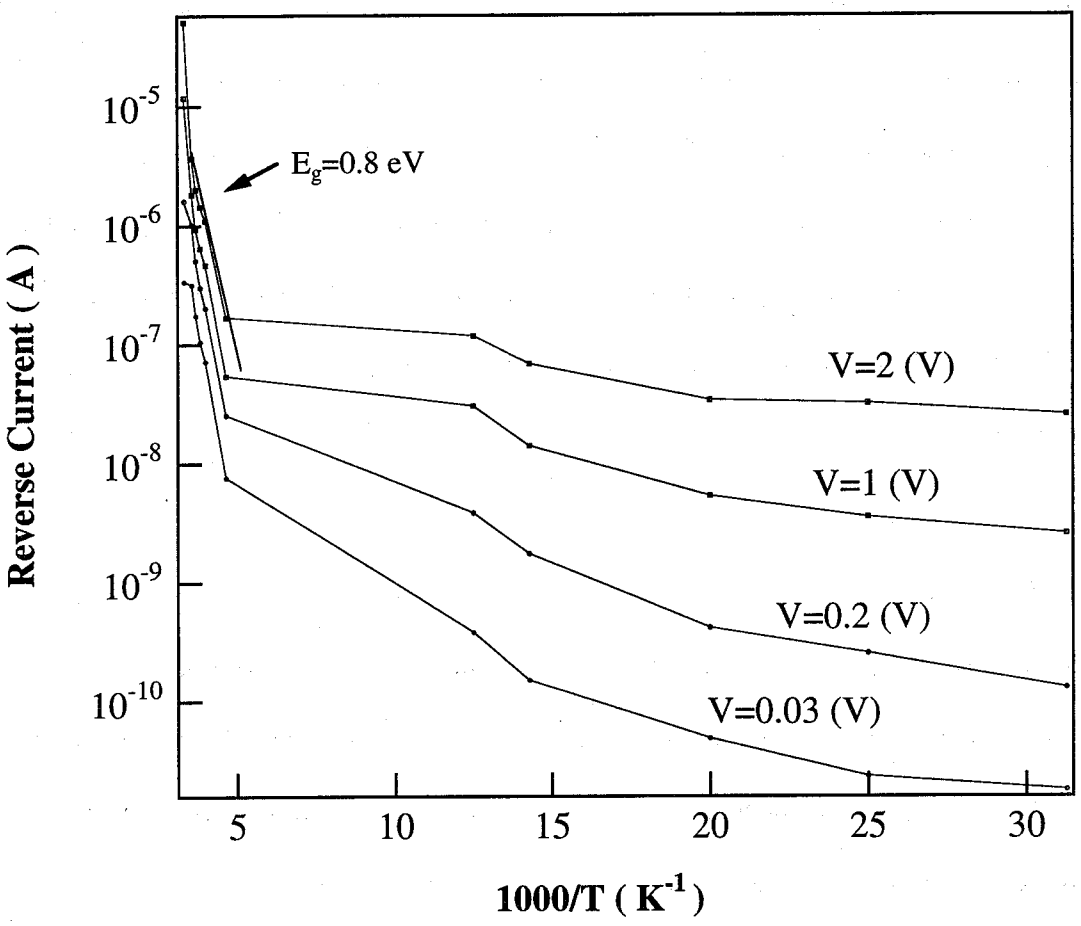

Fig. 3-18 The reverse current versus inverse temperature at different biases.

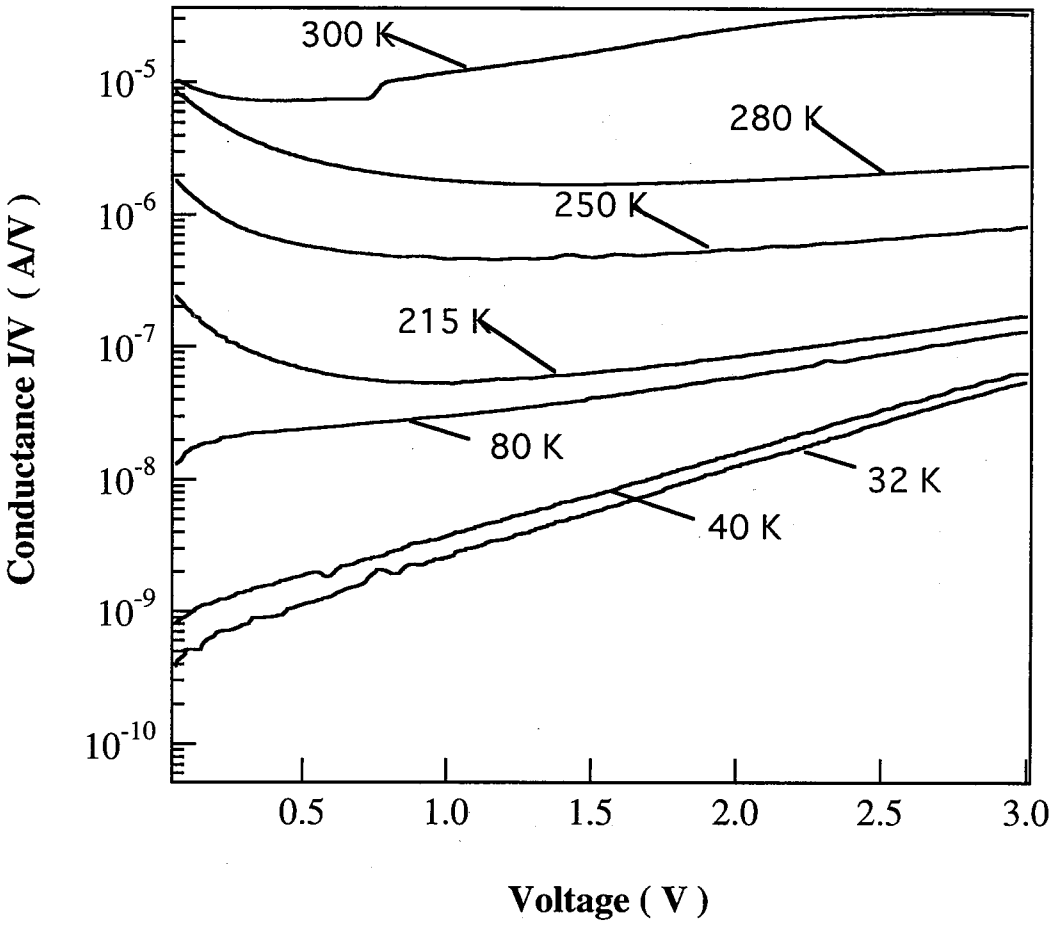

Fig. 3-19 Conductance vs reverse bias voltage at different temperatures.

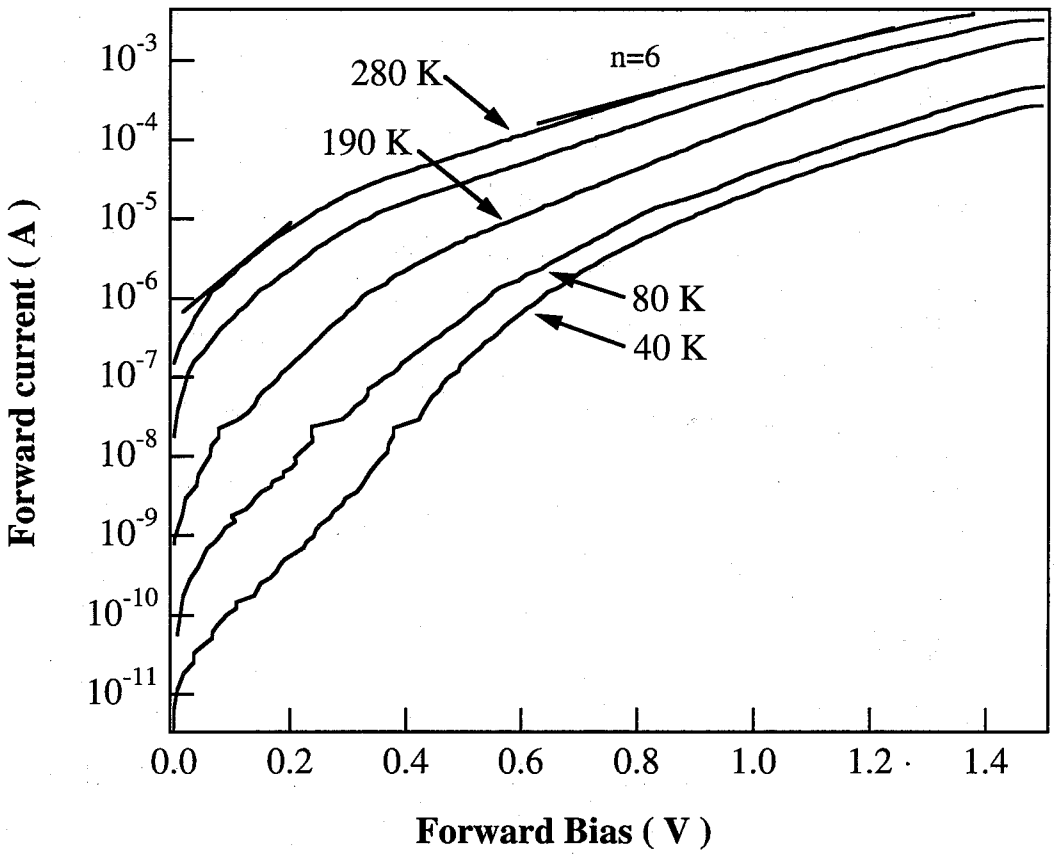

Fig. 3-20 Forward current vs bias voltage at different temperatures.

bias. The variation of the conductance I_R/V_R with the reverse bias V_R is contained in the exponential factor $\exp(1+V_R/V)$. The semilog plots of the I_R/V vs. V of tunnel current should be straight line, the result were shown in Fig. 3-19. When temperature below 280 K, at very large bias region the tunnel current is dominant. And above 215 K the thermal diffusion current are dominant.

B. Forward current

Figure 3-20 shows the results of forward currents vs. bias voltage at different temperatures. At low bias, a temperature-independent slope is observed, It means tunnelling current is dominant.

With temperature increasing, the space recombination current and diffusion current shift to lower bias, and surpass the tunneling current, these currents are masked by series-resistance effects. As temperature increasing up to 300 K, the thermal diffusion current becomes dominant. From the Fig. 3-19 and Fig. 3-20 we can conclude that the tunnel current is important source of dark current for GaSb p-n junction at lower temperature, which may be due to high unintentionally doped, and the Te doped GaSb concentration. a large ideality factor was obtained at high bais voltage, it was caused by the presence of series resistance.[44]

3.7. Conclusions

Variable temperature, Hall-effect measurements have been carried out on several undoped GaSb samples grown by MBE. It is found that the electrical properties of GaSb epilayers strongly depend on growth temperature. High residual impurity concentration and high compensation ratio are observed for lower and higher growth temperatures, respectively. In such samples the residual impurity conduction may be a dominant conduction mechanism at low temperatures, and the common method of curve fitting to concentration vs. $1/T$ curve may give wrong results; therefore, the analysis of mobility vs. T data has been carried out. In addition, the electrical transport properties of GaSb are analyzed in energy dependent relaxation scattering processes and it is demonstrated that device usage of GaSb is limited by high residual impurity concentration as well as high compensation ratio.

PL spectra, a sherp line at 777.5 meV which is due to residual A, and a exciton bound to donor (D) is clearly seen, these implies that our samples, which grown at higher temperature (500°C), have very good crystal quality, because the bound energy of donor exciton is very small for this material.

The temperature dependent I-V characteristics in bulk of GaSb p-n junctions are measured and analyzed. At reverse bias, the tunnel current is dominant at a large temperature region. The large leakage current is mainly caused by tunnel current. The diffusion current surpasses the tunnel current at high temperature and high bias of both forward and reverse voltage.

Appendix

The formulae used to calculate the different scattering mechanisms are taken from the ref. 6 with some corrections. Equation (9) of ref. 6 is,

$$\tau_k = 1/s_{ii}^k + 1/s_{if}^k$$

This equation is changed to

$$\tau_k = \frac{1}{s_{ii}^k + s_{if}^k}$$

which is the correct form.

To calculate ionized impurity scattering, the following formula is used

$$s_{if} = \frac{N_i e^4 m_f^* k_f}{2\pi\varepsilon^2\hbar^3 k_i^4} \int_{-1}^{1} \frac{(1-y)G(y)}{\left[1 + m_f^*/m_i^* - 2\left(m_f^*/m_i^*\right)^{1/2} y + \lambda_D^{-2} k_i^{-2}\right]^2} dy$$

This equation is the same as eq. (A6) of ref. 6 if we assume that light and heavy holes have the same effective mass, but in our case m_1=6m_2, while m_1= m_2 is not a reasonable assumption.

References

[1]D. C. Look, Electrical Characterization of GaAs Materials and Devices (Wiley, New York, 1998).

[2]P. Blood, J. W. Orton, The electrical characterization of semiconductors, Rep. Prog. Phys., 41, 157, (1978).

[3]B. R. Nag, Electron Transport in Compound Semiconductors, Springer-Verlag, Berlin (1980).

[4]D. C. Look, D. K. Lorance, J. R. Sizelove, C. E. Stutz, K. R. Evans, and D. W. Whitson, J. Appl. Phys. **71**, 260 (1992).

[5]J. D. Wiley, in *Semiconductors and Semimetals*, edited by R. K. Willardson and A. C. Beer (Academic, New York, 1975), Vol. 10, Chap. 2.

[6]M. Wenzel, G. Irmer, and J. Monecke, J. Appl. Phys. **81**, 7810 (1997).

[7]M. Costato and L. Reggiani, Phys. Stat. Sol. (b) 58, 47 (1973).

[8]J. D. Wiley, Phys. Rev. B4, 2485 (1957).

[9]E. O. Kane, J. Phys. Chem. Solids 1, 249 (1957).

[10]K. Saito, E. Tokumitsu, T. Akatsuka, M. Miyauchi, T. Yamada, M. Konagai, and K. Takahashi, J. Appl. Phys. 64, 3975 (1988).

[11]Dutta, Bhat, and Kumar, J. Appl. Phys., 81, 5822 (1997).

[12]For a recent review, see A.G. Milnes and A.Y. Polyakov, Solid-State Electron. **36**, 806 (1993).

[13]G R Johnson, B C Caventt, T M Kerr, P B Kirby and C E C Wood, Semicond. Sci. Technol. **3**, 1157 (1988).

[14]C. D. Kourkoutas, P. D. Bekris, G. J. Papaioannou and P. C. Euthmiou, Solid State Commun. **49**, 1071 (1994).

[15]M. E. Lee, D. J. Nicholas, K. E. Singer, and B. Hamilton, J. Appl. Phys. **59**, 2895 (1986)

[16]A. Ya. Vul', G. L. Bir, and Yu. V. Shmartsev, Sov. Phys. Semicond. **4**, 2005 (1971)

[17]M. E. Lee, I. Poole, W. S. Truscott, I. R. Cleverley, and K. E. Singer, J. Appl. Phys. **68**, 131 (1990).

[18]P. S. Dutta, V. Prasad, and H. L. Bhat, J. Appl. Phys. **80**, 2847 (1996).

[19]B. K. Ridley, in *Quantum Processes in Semiconductors* 3rd ed. (Oxford Science, 1993), Chap.6.

[20]M. H. Maaren, J. Phys. Chem. Solids **27**, 472 (1966).

[21]H. N. Leifer and W. C. Jr. Dunlap, Phys. Rev. **95**, 51 (1954).

[22]G. Benoit and P. Lavallard, J. Phys. Chem. Solids **31**, 411 (1970).

[23]R. D. Baxter, R. T. Bate and F. J. Reid, Phys. Chem. Solids **26**, 41 (1964).

[24]K. Nakashima, Japan. J. Appl. Phys. **20**, 1085 (1989).

[25]J. S. Blakemore, Semiconductor Statistics (Pergamon, New York, 1962).

[26]D. C. Look, P. C. Colter, Phys. Rev. **B24**, 1153 (1983).

[27]F. Meinardi, A. Parisini and L. Tarricone, Senicond. Sci. Technol. **8**, 1985 (1993).

[28]M. Lee, D. J. Nicholas, K. E. Singer, and B. Hamilton, J. Appl. Phys. **59**, 2895 (1986).

[29]A. Baraldi, C. Ghezzi, R. Magnanini, A. Parisini, L. Tarricone, A. Bosacchi, S. Franchi, V. Avanzini and P. Allegri, Materials Science and Engineering **B28**, 174 (1994).

[30]C. W. Turner, S. J. Eglash and A. J. Strauss, J. Vac. Sci. Technol. **6**, 45 (1993).

[31]F. Auzel. Proc. IEEE **61**, 758 (1973).

[32]R. A. Noack, W. Ruhle and T. N. Morgan, Phys. Rev. **B5**, 4900 (1972).

[33]D. J. Nicholas, M. Lee, B. Hamilton and K.E. Singer, J. Crystal Growth, **81**, 298 (1987).

[34]W. Jakowetz, W. Ruhle, K. Breuninger and M. Pilkuhn, Phys. Status Solidi, a**12**, 169 (1972).

[35]W. Ruhle, W. Jakowetz, C. Wolk, R. Linnebach and M. Pilkuhn, Phys. Status Solidi, b**73**, 255 (1976).

[36]M. Lee, D. J. Nicholas, K. E. Singer and B. Hamilton, J. Appl. Phys. **59**, 2256 (1986).

[37]E. H. Rhoderick and R. H. Williams, *Metal-Semiconductor Contacts* (Clarendon, Oxford, 1988).

[38]D. K. Shroder, *Semiconductor Material and Device Characterization* (Wiley, New York, 1990).

[39]S. M. Sze, *Physics of Semiconductor Devices* (Wiley, New York, 1981).

[40]S. M. Sze, *Physics of Semiconductor Devices* (Wiley, New York, 1969).

[41]J. F. Chen and A. Y. Cho, J. Appl. Phys. **70**, 277 (1991).

[42]E. O. Kane, J. Appl. Phys. 32, 83 (1961).

[43]T. A. Demassa and D. P. Knott, Solid-State Electron. **13**, 131 (1970).

[44]F. H. Mitchell, Electron. Ind. **10**, 96 (1961).